IEEE Access
Multidisciplinary ⋮ Rapid Review ⋮ Open Access Journal

Received 24 July 2025, accepted 27 August 2025, date of publication 8 September 2025, date of current version 19 September 2025.

Digital Object Identifier 10.1109/ACCESS.2025.3607095

TOPICAL REVIEW

Recent Advances in Transparent Reflectarray Antennas

ALTAF AHMED MUGHERI[1], MUHAMMAD INAM ABBASI[1], (Senior Member, IEEE), IMRAN MOHD IBRAHIM[1], (Senior Member, IEEE), SAAD HASSAN KIANI[1], MUHAMMAD HASHIM DAHRI[2], MUHAMMAD RAMLEE KAMARUDIN[3], (Senior Member, IEEE), ZAID AHMED SHAMSAN[4], (Senior Member, IEEE), AND QAMMER HUSSAIN ABBASI[5], (Senior Member, IEEE)

[1]Faculty of Electronics and Computer Engineering and Technology (FTKEK), Universiti Teknikal Malaysia Melaka (UTeM), Hang Tuah Jaya, Melaka 76100, Malaysia
[2]Department of Electronic Engineering, Dawood University of Engineering and Technology, Karachi, Sindh 74800, Pakistan
[3]Faculty of Electrical and Electronic Engineering, Universiti Tun Hussein Onn Malaysia, Batu Pahat, Johor 86400, Malaysia
[4]Department of Electrical Engineering, College of Engineering, Imam Mohammad Ibn Saud Islamic University (IMSIU), Riyadh 11432, Saudi Arabia
[5]James Watt School of Engineering, College of Science and Engineering, University of Glasgow, G12 8QQ Glasgow, U.K.

Corresponding authors: Muhammad Inam Abbasi (inamabbasi@utem.edu.my) and Muhammad Ramlee Kamarudin (mramlee@uthm.edu.my)

The study is funded by the Ministry of Higher Education (MOHE) of Malaysia through the Fundamental Research Grant Scheme (FRGS), No. FRGS/1/2023/TK07/UTEM/02/7. Communication of this research is also made possible through monetary assistance by Universiti Tun Hussein Onn Malaysia and the UTHM Publisher's Office via Publication Fund E15216.

ABSTRACT Transparent Reflectarray Antennas (TRAs) have emerged as a promising solution for next-generation communication systems requiring both electromagnetic performance and optical transparency. This review focuses on a detailed latest work on unit cell design innovations, material engineering, and performance optimization across microwave, millimeter-wave, and terahertz frequency bands. Key developments include the use of fine metal lines (FML), frequency selective surfaces, indium tin oxides (ITO) films, and liquid crystal-based reconfigurable structures to achieve wide phase tuning, low reflection loss, and high transmittance. Various fabrication techniques, such as photolithography on quartz and soda-lime glass substrates, have enabled lightweight and high-efficiency RA structures suitable for integration into smart windows, satellite platforms, and 6G communication devices. Additionally, transparent beam-steering mechanisms using anisotropic liquid crystal (LC) materials and metallic mesh frameworks demonstrate the feasibility of dynamic control while maintaining optical clarity. The paper also discusses current challenges—such as optical loss, material limitations, and fabrication complexity—and outlines future directions aimed at enhancing bandwidth, reconfigurability, and multifunctional performance of TRAs.

INDEX TERMS Transparent reflectarray antenna, transparent materials, mm-wave, frequency selective surfaces.

I. INTRODUCTION

Transparent antennas are attracting growing interest due to their ability to transmit electromagnetic signals while remaining optically invisible, offering seamless integration into various surfaces. These antennas can be mounted in smartphone screens, glasses, human bodies, and building windows without affecting the surrounding environment. Transparent Reflectarray Antennas (TRA) represent a promising direction in the evolution of Reflectarray (RA) designs, with potential applications in multiple modern communication systems. These antennas are especially valuable for use in satellites and wireless communication systems to achieve high optical transmittance [1], [2], [3], [4], [5]. TRAs hold strong potential

The associate editor coordinating the review of this manuscript and approving it for publication was Sudipta Chattopadhyay.

© 2025 The Authors. This work is licensed under a Creative Commons Attribution 4.0 License.
For more information, see https://creativecommons.org/licenses/by/4.0/

for future research, particularly for applications requiring both transparency and performance, such as solar-powered systems, windows for uncrewed aerial vehicles (UAVs), and integrated antenna systems on buildings. By allowing light transmission, TRAs can be combined with solar panels or placed on transparent surfaces in vehicles and infrastructure. Furthermore, optically transparent designs open the door to more innovative applications with the use of advanced materials [6], [7], [8], [9], [10], [11], [12], [13]. The design of TRAs incorporates strategies such as combining single and multi-resonance modes for phase variation control and selecting low-loss dielectric materials as substrates. Materials like glass are preferred due to their optical clarity and favorable dielectric properties. Proper selection of dielectric constant and loss tangent is essential for ensuring good antenna performance. Meanwhile, the patch elements often use Transparent Conducting Oxides (TCOs) [14], [15], [16], [17] with Indium Tin Oxide (ITO) [18], [19] being one of the most widely used alternatives to conventional metallic conductors. However, one of the main challenges in using ITO is its relatively high conductor loss, which can negatively impact the efficiency of the antenna.

The design of TRA typically incorporates meshed elements, where maintaining an optimal mesh density is crucial. Implementing appropriate gaps between mesh lines helps to preserve performance, as overly thin meshes can degrade antenna efficiency. This paper analyzes various materials used for both substrates and conductors. Glass is one of the most commonly used substrate materials in existing studies, often paired with Indium Tin Oxide (ITO) [20], [21], [22], [23], [24] or combined with composite materials to enhance both optical transparency and antenna gain. However, because ITO's electrical conductivity is significantly lower than that of conventional metals like copper [25], conductor losses become a critical factor. These losses and their impact on antenna performance are investigated across several studies and discussed in detail in later sections.

This review also explores a wide range of transparent materials, detailing the dielectric and conductive properties—such as dielectric constant, loss tangent, and conductivity—used in various transparent antenna designs. Examples include AZO/silver nanowire stacked films in [26] AgHT-based conductors [27], [28], [29], [30], [31], graphene-based materials [32], [33], [34], [35], [36], [37] and micro-metal mesh conductive films [27], [38], [39], [40], Other unique approaches include the use of distilled water as a dielectric medium [41], [42], [43], multilayer film antennas, and fluorine-doped tin oxide (FTO) coatings [8], [44], [45], [46]. Many of these designs operate in the Ka band and higher frequency ranges, including dual-band implementations [47], [48], [49], [50], [51]. The summarized technical details of each work—such as antenna operating frequency, gain, dimensions, radiation efficiency, bandwidth, dielectric constant, conductivity, and transparency—are presented in Table 1.

This review aims to support the future development of TRAs, particularly in applications requiring transparency and compact form factors, such as CubeSats for satellite communication, UAVs, and smart city/IoT devices. Section II provides an in-depth overview of transparent materials with comparative tables; Section III discusses TRA design approaches and their applications; and Section VI concludes the paper.

II. MATERIALS USED FOR TRANSPARENT ANTENNAS

It is essential to explore all available materials to identify the most suitable options for designing TRAs. Therefore, this paper presents a comprehensive analysis of various materials, summarizing the structural elements and design parameters used in existing literature. Table 1 offers a detailed comparison of different transparent antenna designs, focusing on key performance indicators and material characteristics.

The parameters highlighted in the table include operating frequency, transparency level, antenna gain, bandwidth, dielectric and conductor materials, radiation efficiency, and physical dimensions. These parameters provide valuable insights into the trade-offs between transparency and performance, while also reflecting the innovation in materials and fabrication techniques adopted in recent studies.

This comparative analysis in Table 1 serves as a practical guide for understanding the progress in TRA development and aids in the selection of materials that offer both high conductivity and optical transparency.

A detailed comparative analysis of transparent antennas developed across a broad range of frequency bands, emphasizing their physical dimensions, electrical characteristics, material properties, and optical transparency. Key antenna parameters presented include operational frequency, gain, physical dimensions normalized to wavelength (λ), aperture efficiency, fractional bandwidth, dielectric constant (ε_r) along with loss tangent ($\tan\delta$), type of conductor, and percentage of optical transparency. This collection of data offers important insights into how various combinations of materials and design strategies influence antenna performance, particularly in scenarios where both radio-frequency functionality and visual transparency are required.

From the analysis [122] meta material enhanced glass surface in TR, it is observed that antennas designed for mmWave frequencies—such as 28 GHz and 60 GHz—exhibit notably compact sizes, often less than 0.2λ, while maintaining directional radiation characteristics and acceptable gain levels. This is especially prominent in configurations using substrates like borosilicate glass, quartz, or PDMS in conjunction with transparent conductive materials such as Indium Tin Oxide (ITO), Fluorine-doped Tin Oxide (FTO), or AgHT-8 films. ITO-based designs, in particular, demonstrate consistent performance, offering high gain values (typically in the 19–27 dBi range) alongside excellent transparency (ranging from 80% to 92%), making them ideal candidates for integration in modern transparent surfaces such as smart displays, building facades, and vehicle windows. Conversely, antennas operating in lower frequency bands (1.26–5.85 GHz) tend

TABLE 1. Detailed materials used in transparent antennas with parameters.

Frequency (GHz)	Gain (dBi)	Physical Dimension (λ^2)	Aperture Efficiency (%)	Bandwidth (%)	Dielectric Constants (substrate)	Conductor (patch material)	Transparency (%)
27.5 /29.5 [32]	19.5	0.243 x 0.212	32.3 & 75.9	8.8	RO3003 (ε_r=3, tanδ=0.0010)	ITO (1.3 x 10^4 S/cm)	92
1.26 [54]	1.66	0.193 x 0.151	52-54	10	Polymide (ε_r =3.5, tanδ= 0.008)	IZTO/Ag/IZTO (σ=3.96 x 10^6 S/m)	86
2.47 / 5.32 [55]	0.64/1.2	0.4 x 0.4	62 and 83	7.15/2.42	Borosilicate glass (ε_r =4.6, tanδ=0.008)	AgHT-8 (σ=1.25 × 10^5 S/m)	80
2.44 / 5.5 [38]	0.74/2.30	2.67 x 0.67	40	10.20 / 5.12	Glass	MMC (Micro metal Mesh Conductive)	75
2.45/ 5.8 [56]	4.94	0.504 x 0.546	N/A	2.2	Quartz (ε_r =3.80, tanδ= 0.0015)	AgHT-8 (σ=1.25 × 10^5 S/m)	95.9
60 [57]	12.5	1.4 x 2.2	N/A	10	Au/GL- Gold grid layer (ε_r =6.9, tanδ=0.0001)	AgHT-8 (σ=1.25 × 10^5 S/m)	74.6
20 [58]	19	1.33 x 2.0	N/A	N/A	Polymer substrate (ε_r =2.55, tanδ=0.002)	Silver bus bar (6.2×10^7 S/m)	N/A
28 [59]	25.8	0.119 x 0.107	73	17	borosilicate glass (ε_r =4.6, tanδ=0.008)	ITO (1.3 x 10^4 S/cm)	N/A
20 [60]	27.3	10.67 x 10	40	N/A	Glass	ITO (1.3 x 10^4 S/cm)	81
5.85 [61]	-10	1.014 x 1.014	52	N/A	Metal Substrate (ε_r =4.6, tanδ=0.0036)	ITO (1.3 x 10^4 S/cm)	84
5 [45]	3.63	0.735 x 0.54	74	19.06	Pyrex glass (ε_r =4.6, tanδ=0.0037)	FTO (Flourine doped Tin oxide)	90
58 / 59.7 [62]	13.6/ 15.6	4.65 x 4.95	60	N/A	PET (Polyethylene-terephthalate)	Silver layer (6.2×10^7 S/m)	68/ 87
10 [63]	10	1.33 x 1.33	N/A	125	PET (ε_r =3.80, tanδ= 0.0015)	ITO (1.3 x 10^4 S/cm)	N/A
2.43 [64]	1.66	0.373 x 0.243	54	10	Polymide (ε_r =3.5, tanδ= 0.003)	IZTO/Ag/IZTO (σ=3.96 x 10^6 S/m)	86
2.7 [65]	4	1.08 x 2.69	82	35	Plexiglass (ε_r =3.4)	Distilled water (σ=0.5 to 3 µS/cm)	N/A
60 [66]	12	3.2 x 2.8	N/A	N/A	Glass	ITO (1.3 x 10^4 S/cm)	75
1.98 [42]	0.25	0.079 x 0.040	72	35	Water patch ethyl acetate, also used Air (ε_r =1.005)	Distilled water (σ=0.5 to 3 µS/cm)	100
5.52 [67]	22.16	0.4 x 0.4	53.14	4.42	Glass	AgHT-8 and copper	N/A
43.8 [68]	1.83	1.46 x 1.75	90.57	58.7	Plexiglass (ε_r =3.4)	AgHT-8 (σ=1.25 × 10^5 S/m)	N/A
2.4 [69]	13.97 dB	0.376 x 0.020	N/A	16.35	Sapphire wafer done on silica glass	GZO (Gallium doped Zinc oxide) (σ=1408 S/cm)	N/A
5.85 [70]	5.44	0.8 x 1.5	N/A	40.38	Cellulose acetate (ε_r =6.4, tanδ=0.0097)	ITO (1.3 x 10^4 S/cm)	N/A

TABLE 1. (*Continued.*) **Detailed materials used in transparent antennas with parameters.**

29 [71]	N/A	1.35 x 2.18	N/A	N/A	c-sapphire substrate (ε_r =9.3,tanδ=0.0003 perpendicular to c-axis), (Er=11.5,tanδ=0.00086 parallel to c-axis)	GZO (Gallium doped Zinc oxide) (σ=1.4 x 10^3 S/cm)	90
6 [72]	3.63	1 x 0.8	N/A	N/A	PDMS (Polydimethyl siloxane) (ε_r =2.4, tanδ=0.06)	woven meshed fabric coated with nickel/zinc blackened copper	90
26 [73]	22.9	0.924 x 0.374	N/A	15	Solar cell backed gold plated	ITO (σ=1.3 x 10^4 S/cm)	N/A
780 [74]	2.84	N/A	56.45	10	Polymide (ε_r r=3.5, tanδ= 0.008)	FTO (Flourine doped Tin oxide)	80
4.9 [75]	5.14	0.327 x 0.556	90	N/A	Soda lime glass (ε_r =7.3, tanδ=0.02)	FTO (Flourine doped Tin oxide)	80
2.4 [26]	1.3	N/A	90	N/A	Plexiglass (ε_r =3.4)	AZO/AgNWs (Aluminum doped zinc oxide/Silver Nanowires) (σ=752 S/cm)	80.28
27.5-29.5 [76]	3	N/A	N/A	8.8	PMMA (Polymethyl/methacrylate) (ε_r =3.9, tanδ=N/A	ITO (σ=1.3 x 10^4 S/cm)	80
23.5 – 32 [77]	12.1	7.89 x 16	N/A	N/A	Rogers RT5880, rear glass (ε_r =2.2, tanδ=0.02)	ITO (σ=1.3 x 10^4 S/cm)	80
2.45 [78]	10	N/A	52	N/A	PET (ε_r =3, tanδ=0.002) Microstrip R03003	AgNw (Silver nanowire) (σ=6.3 × 10^7 S/m)	85
26 [79]	0.37	N/A	N/A	N/A	PDMS (Polydimethyl siloxane) (ε_r =2.4, tanδ=0.06)	AgNw (σ=8.13x10^5)	85

to exhibit larger physical sizes relative to the wavelength; however, the use of high-permittivity or low-loss dielectric substrates contributes to more efficient miniaturization and improved impedance characteristics.

The table further highlights the inherent trade-offs between bandwidth and gain. Antenna designs that achieve broader bandwidths—typically greater than 15%—often do so at the expense of reduced aperture efficiency or higher conductor losses. These trade-offs are particularly relevant for applications demanding high data rates, such as 5G and future 6G networks, where wideband performance is essential. Substrate materials such as polyimide, PET, and Plexiglass are commonly employed due to their flexibility, low dielectric losses, and suitability for roll-to-roll fabrication or printed electronic processes.

The choice of conductive material also plays a critical role in determining both radio-frequency (RF) and optical characteristics. While materials like silver nanowires (AgNW) and gallium-doped zinc oxide (GZO) provide excellent transparency and electrical conductivity, they may present challenges in terms of cost or mechanical durability when compared to more widely used alternatives such as Indium Tin Oxide (ITO).

It is also important to point out that several designs in the literature lack complete reporting of essential parameters like aperture efficiency or normalized physical dimensions. This inconsistency underscores the need for more standardized evaluation methods within the field of transparent antenna research. Nevertheless, the data in the table illustrates that high-performance transparent antennas are achievable by optimizing the interplay between dielectric and conductive materials. The most effective designs demonstrate gains exceeding 10 dBi, bandwidths over 10%, and optical transparency greater than 85%, thus successfully meeting the dual demands of electromagnetic performance and visual invisibility.

In conclusion, Table 1 encapsulates the ongoing advancements in transparent antenna technology, emphasizing the pivotal role of material selection and miniaturization techniques. The comparative insights gathered from this analysis provide a solid foundation for designing next-generation transparent RF systems. These findings are particularly rel-

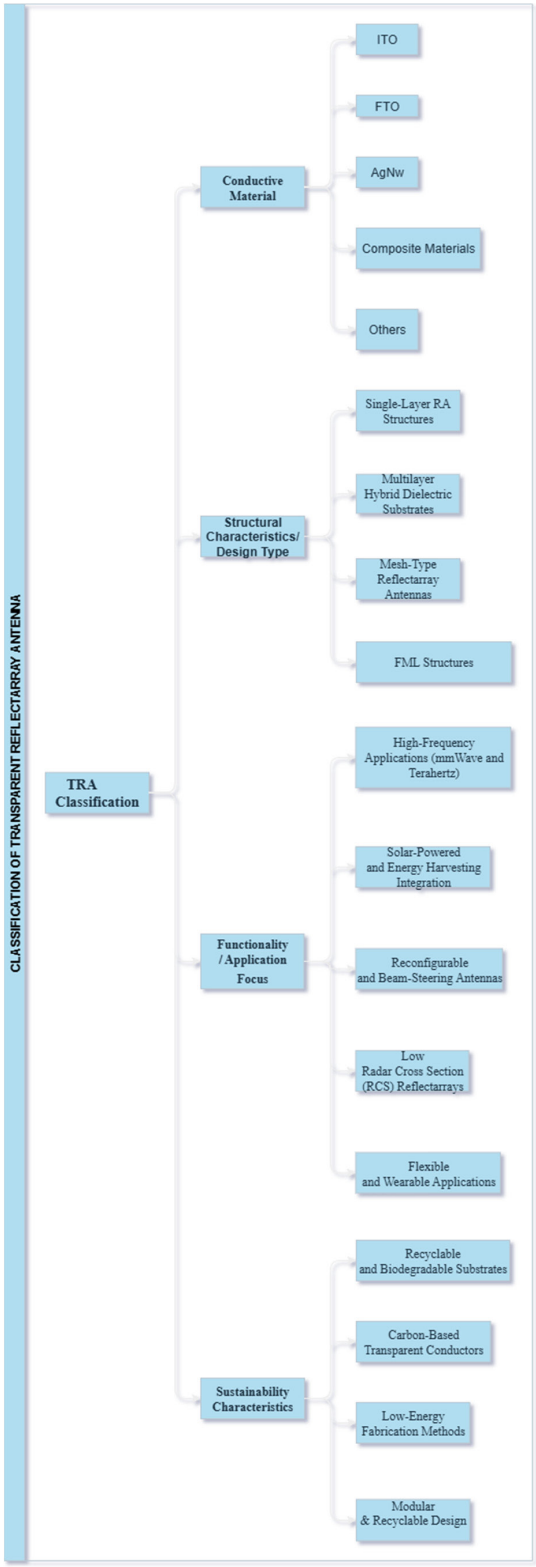

FIGURE 1. Structural diagram for transparent Reflectarray antenna.

evant for emerging applications such as wearable electronics, vehicular communication platforms, and 6G-enabled intelligent environments, where optical transparency must coexist with high-performance wireless functionality.

A. USING AgHT-8 AS CONDUCTOR

The term ''transparent'' typically refers to materials such as glass or crystal, which are widely suitable for research and integration in environments where optical clarity is essential. In recent literature, various materials and their properties have been explored for the development of transparent antennas. The selection of both substrate and conductor materials plays a critical role in achieving desired antenna performance. Key parameters to consider include electrical conductivity, loss tangent, and dielectric constant. As highlighted in Table 1, AgHT-8—a silver-coated transparent film—demonstrates a light transmittance of approximately 88% [27] It achieves a gain of 0.64 dBi at 2.46 GHz and 1.2 dBi at 5.32 GHz, with radiation efficiencies of 62% and 83%, respectively, when using borosilicate glass as the dielectric substrate and attaining 80% optical transparency [53]. Additionally, conductive wire grids comprising nanoscale to mesoscale metal wires have been implemented in various configurations. These wire grid structures are fabricated using commercially available chemical vapor deposition (CVD) and photolithographic techniques. Bulk copper (Cu) and translucent polyethylene terephthalate (PET) surfaces are typically processed through wet etching. In this context, PET films with a thickness of 50 μm have been utilized as insulating layers; however, their influence on the electrical performance of transparent antennas becomes minimal when film thickness falls below the submillimeter range. Notably, similar performance—gain of 0.64 dBi at 2.46 GHz and 1.2 dBi at 5.32 GHz, with 62% and 83% radiation efficiency—was achieved using borosilicate glass substrates and 80% transparency [54].

An optically transparent microstrip (OTM) patch antenna array has been designed, analyzed, and experimentally validated for 60 GHz applications [55], [59], and [65]. The antenna utilizes a two-layer mesh configuration optimized to reduce ohmic losses in the feeding network while achieving an optical transparency of up to 74.6%. Numerical parametric studies indicate that the misalignment between the two mesh layers significantly influences both optical transparency and electromagnetic performance. Practical design guidelines for mesh alignment and integration are also presented. The measured performance of the OTM antenna closely aligns with that of its opaque counterpart, exhibiting comparable gain and radiation characteristics, thereby validating the transparent design approach [55]. A related study investigates a multilayer printed transparent antenna using an Au/GL (gold grid layer) as the dielectric substrate. Additionally, a transparent antenna based on AgHT-8 film has been fabricated, simulated, and measured. When compared to reference antennas made with AgHT-4 and conventional copper, the AgHT-8-based antenna demonstrates superior transparency and favorable performance in terms of return loss and radiation efficiency. The radiation pattern resembles that of a dipole, with directed radiation, and shows

TABLE 2. Comparison of AgHT-8 material-based transparent antenna designs.

Antenna Type/ References	Structural Characteristics / Design Types	Key Differences/ Technical Insights
Single-layer AgHT-8 Transparent Antenna	- Conductor: AgHT-8 silver-coated transparent film - Borosilicate glass - 2.46 GHz and 5.32 GHz	- Achieved gains of 0.64 dBi at 2.46 GHz and 1.2 dBi at 5.32 GHz - Radiation efficiency: 62% and 83% - Transparency: ~80% - Suitable for low-profile wireless applications such as WLAN and ISM bands
AgHT-8/ AgHT-4/ Copper Antenna [67]	- Compared antennas fabricated using AgHT-8, AgHT-4, and conventional copper - 3.68 GHz and 5.52 GHz - Meandered patch dipole design	- AgHT-8 showed better transparency and comparable efficiency - Impedance Bandwidth: 10.2% (3.68 GHz), 5.12% (5.52 GHz) - Supports IEEE 802.11a and WiMAX M3500T-01/04 standards - Performance closely resembled dipole-type radiation patterns
Wideband Transparent Antenna for 5G [80]	- Substrate: Plexiglass (ε_r = 3.4)- Refined patch shape to optimize bandwidth- Conductor: Presumed AgHT-8 or similar transparent film	- Achieved wide impedance bandwidth from 23.92 GHz to 43.8 GHz - Well-matched simulated and measured results for gain, return loss, and patterns - Designed for high-speed 5G communication systems
OTM Patch Antenna Array, [57], [62], [68]	- Dual-layer mesh configuration- Feeding network optimized to reduce ohmic losses- Uses Au/GL gold grid on dielectric glass	- Optical transparency up to 74.6% - Similar performance to opaque reference antennas - Mesh misalignment sensitivity analyzed - Design guidelines provided for multilayer transparent mesh networks

TABLE 3. Comparison of Silver and Silver Nanowire material-based transparent antenna designs.

Antenna Type/ References	Structural Characteristics / Design Types	Key Differences and Technical Insights
Broadband Transparent Antenna with Silver Bus Bar [58]	- Substrate: Polymer (ε_r = 2.55) - Conductor: Silver bus bar - Wideband design	- Operates from 0.5 GHz to 16.7 GHz- Gain varies from 3 dB to 19 dB - Low optical shadowing, suitable for solar panel integration
Transparent 4×2 Patch Array at 60 GHz [62]	- Substrate: PET - Radiator & ground: Double-sided micrometric silver mesh - Compared with opaque silver reference	- Transparent array shows resonance shift of 3.6 GHz (from 59.7 GHz)- Gain: 11.6 dBi vs. 15.6 dBi (opaque) - Maintains structural transparency, but slightly reduced performance
Screen-Printed AgNW Antenna [78]	- Substrate: Rogers R03003 PET - Conductor: Silver nanowire (AgNW) - Fabrication: Screen printing	- Achieves >85% transparency- Radiation efficiency ~50% - Suitable for transparent RFID, automotive, and aerospace applications - Scalable, low-cost printing method
PDMS-based Transparent Antenna [79]	- Substrate: PDMS (flexible polymer) - Frequency: 26 GHz - Transparent conductive layer unspecified, assumed AgNW or similar	- 85% optical transparency - Designed for mmWave applications - Suitable for flexible and stretchable antenna systems in wearable or window-based applications

efficiency improvements without significantly compromising antenna performance. The impedance bandwidths achieved are 10.20% at 3.68 GHz and 5.12% at 5.52 GHz, effectively covering the IEEE 802.11a and WiMAX M3500T-01/04 (3.4–3.8 GHz) standards [64]. Moreover, a thin, optically transparent wideband antenna designed for high-speed 5G communications has been proposed and studied [76]. By optimizing the geometry of the patch, the antenna achieves a wide impedance bandwidth ranging from 23.92 GHz to 43.8 GHz. Its measured return loss, radiation patterns, and gain align closely with simulated results, confirming its applicability for mmWave 5G applications. The design employs Plexiglass as the dielectric substrate, characterized by a relative permittivity of 3.4.

Following Table 2 highlights the AgHT-8 material type antennas:

B. SILVER AND SILVER NANOWIRE(AGNW)

The antenna proposed in [56] demonstrates wideband characteristics suitable for supporting multiple wireless technologies while maintaining a minimal shadowing footprint, thereby preserving the efficiency of integrated solar panels. The design utilizes a polymer substrate with a relative permittivity (ε_r) of 2.55 and a silver bus bar as the conductive element. It operates across a broad frequency range from 0.5 GHz to 16.7 GHz, with a reported gain spectrum varying from 3 dBi to 19 dBi, as summarized in Table 1. Furthermore, a 4 × 2 microstrip patch antenna array with optical transparency was designed, fabricated, and tested in [59] This antenna employs double-sided micrometric mesh silver films as the conductive layers and a polyethylene terephthalate (PET) substrate as the dielectric, operating effectively at 60 GHz. Compared to its opaque reference counterpart, which used continuous silver films and achieved a gain of 15.6 dBi at 59.7 GHz, the transparent version exhibited a

TABLE 4. Comparison of Indium Tin Oxide (ITO) material-based transparent antenna designs.

Antenna Type/ References	Structural Characteristics / Design Types	Key Differences and Technical Insights
ITO with Rogers R03003 Substrate [49]	- Substrate: Rogers R03003 - Frequency: 27.5–29.5 GHz - Transparency: 92%	- Achieved gain of 19.5 dBi - High optical transparency (>90%) - Suitable for mmWave high-data-rate applications.
ITO with Glass / Borosilicate Substrate [59], [60], [66]	- Substrates: Glass and Borosilicate Glass - Frequencies: 20 GHz, 28 GHz, 60 GHz - Transparency: ~82%	- Gain decreases with increasing frequency (from 27.3 dBi to 12 dBi) - Radiation efficiency up to 73% - Suitable for wide-frequency applications with acceptable trade-offs.
ITO with Metal Substrate [61]	- Dielectric constant: 4.6 - Loss tangent: 0.0036- Frequency: 5.85 GHz - Transparency: 84%	- Low-frequency ITO application - Balances metal support with moderate transparency - Useful for robust, hybrid reflective surfaces.
ITO with PET Substrate [63]	- Substrate: PET (flexible polymer) - Frequency: not specified	- Suitable for flexible transparent systems - Good trade-off between mechanical flexibility and transparency.
ITO with Gold-plated Substrate [73]	- Frequency: ~26 GHz- Substrate: Gold-coated	- Achieved gain of 22.9 dBi - Potential for high-gain, precision systems in mmWave spectrum.
ITO RA with Extra-Wide Patch Elements	- Design innovation: Extra-wide rectangular patches and subwavelength elements- Frequency: Centered at 20 GHz- Phase range: 272°	- Peak reflection loss: 1.5 dB - Full RA gain: 22.2 dBi, beam at 20° off-broadside - Demonstrates loss-reduction design strategy.
ITO with PMMA and RT5880 Substrates [76], [84]	- Frequencies: 23.5–32 GHz- Transparency: 80%- Gain: 12.1 dBi (RT5880)	- PMMA and RT5880 offer different dielectric support options

resonance frequency shift of 3.6 GHz and a reduced gain of 11.6 dBi. The structure involves conventional mesh patterning techniques applied to both the radiating and ground layers. In [74] screen-printed optically transparent antennas based on silver nanowires (AgNW) were demonstrated using a Rogers R03003 PET substrate. These antennas achieved

TABLE 4. (*Continued*) Comparison of Indium Tin Oxide (ITO) material-based transparent antenna designs.

		- RT5880 ensures low-loss performance at mmWave - Suitable for modular design integration

TABLE 5. Comparison of composite material-based transparent antenna.

Antenna Type/ References	Structural Characteristics / Design Types	Key Differences and Technical Insights
IZTO/Ag/IZTO on Polyimide for Mobile Devices [64]	- Multilayer thin-film: Indium-Zinc-Tin Oxide / Silver / IZTO - Substrate: Polyimide ($\varepsilon_r = 3.5$) - Antenna geometry: Dual branch + connected loop - Center frequency: 2.4 GHz	- Fabricated using DC pulse sputtering - Measured gain: 1.66 dBi - Transparency: 86% - Offers flexibility, low resistivity, and high transparency - Optimized for compact mobile devices.
IZTO/Ag/IZTO with Polyimide [54]	- Similar IZTO/Ag/IZTO multilayer stack - Substrate: Polyimide - Operating frequency: 1.2 MHz	- Gain: 1.66 dBi-Transparency: 86% - Low-frequency application - Suitable for flexible transparent electronics and IoT tags

over 85% optical transparency while maintaining a high radiation efficiency of approximately 50%. Such performance metrics render these antennas highly suitable for integration into commercial transparent platforms, including RFID tags, vehicle-mounted antennas, aerospace windows, and touchscreen devices. Additionally, in [75] presents a transparent antenna fabricated with polydimethylsiloxane (PDMS) as the substrate material, designed to operate at 26 GHz. This design achieves an optical transparency of approximately 85%, making it a viable candidate for high-frequency transparent antenna applications.

Table 3 insights into the comparison of Silver and Silver Nanowire (AgNW) Material-Based Transparent Antennas:

C. INDIUM TIN OXIDE (ITO)

Optically transparent antennas (OTAs) increasingly utilize transparent conductive materials such as ITO, gallium-doped zinc oxide (GZO) [77], fluorine-doped tin oxide (FTO) [78] and indium zinc tin oxide (IZTO) [79] owing to their balanced electrical conductivity and optical transparency. Among these, ITO has been identified as the most effective material for achieving high transparency, frequently surpassing 90%. For example, in [47]. an ITO-based transparent antenna fabricated on a Rogers R03003 substrate operated within the 27.5–29.5 GHz frequency range, achieving a notable gain of 19.5 dBi with an optical transparency of 92%, as detailed in Table 1.

In contrast, ITO antennas reported in [25] which utilize glass or borosilicate glass as substrate materials, demonstrated reduced transparency levels below 90%—approximately 82%—with gains decreasing from 27.3 dBi to 12 dBi as the operating frequency increases from 20 GHz to 60 GHz. Despite this reduction in gain and transparency, the design in where the antenna was designed for operation at a lower frequency of 5.85 GHz. This configuration attained 84% transparency, with the metallic substrate characterized by a dielectric constant of 4.6 and a loss tangent of 0.0036. These studies collectively demonstrate ITO's versatility across various frequency regimes and substrates, reinforcing its position as a leading material for transparent antenna applications.

Furthermore, ITO has also been applied in conjunction with metallic substrates, as in [60] where the antenna was designed for operation at a lower frequency of 5.85 GHz. This configuration attained 84% transparency, with the metallic substrate characterized by a dielectric constant of 4.6 and a loss tangent of 0.0036. These studies collectively demonstrate ITO's versatility across various frequency regimes and substrates, reinforcing its position as a leading material for transparent antenna applications.

In [1] a RA antenna operating at approximately 26 GHz achieved a peak gain of 22.9 dBi using a gold-plated substrate. One of the principal challenges in the design of transparent conductive oxide (TCO) antennas lies in addressing conductor losses, which are often overlooked in conventional RA configurations. To mitigate these losses, the study employed extra-wide rectangular patches along with subwavelength elements in the design of an ITO-based RA. The optimized unit cell demonstrated a phase range of 272° and a peak reflection loss of 1.5 dB. Furthermore, a complete RA prototype incorporating this unit cell achieved a measured peak gain of 22.2 dBi, producing a beam tilted at 20° off-broadside. The results from simulation and experimental validation showed strong consistency, indicating the effectiveness of the proposed design strategy.

Additionally, alternative substrate materials such as polymethyl methacrylate (PMMA) [72] and Rogers RT5880 [80] have been employed in conjunction with ITO to realize transparent antenna structures operating in the 23.5 GHz to 32 GHz frequency range. These implementations attained transparency levels of approximately 80%, with a gain of 12.1 dBi reported for the design utilizing the RT5880

TABLE 6. Comparison of Fluorine-Doped Tin Oxide (FTO) material-based transparent antenna.

Antenna Type/ References	Structural Characteristics / Design Types	Key Differences and Technical Insights
FTO with Pyrex Glass Substrate [45]	- Substrate: Borosilicate (Pyrex) glass - Operating frequency: 5 GHz - Transparency: 90%	- Gain: 3.63 dBi - Good optical and RF performance balance - FTO offers low toxicity, high mechanical strength, and corrosion resistance - Well-suited for integration with solar panels.
FTO-based Transparent Antennas (2.5–5 GHz)	- Substrate: Pyrex glass - Operating band: 2.5 to 5 GHz - Conductor: FTO film	- Designed for multi-band transparent microstrip antennas - FTO on glass supports low dielectric loss and stable environmental performance.
E-Shaped Antenna with TIO on Polyimide [74]	- Conductor: Titanium-doped Indium Oxide (TIO) - Substrate: Polyimide - Frequency: 710–785 GHz (THz band)	- Peak gain: 3.48 dBi @ 730 GHz, gain >2.6 dBi across band - Radiation efficiency: 55–59.78% - Suitable for future THz communication systems. - Achieves 10% impedance bandwidth
FTO on Soda Lime Glass [75]	- Substrate: Soda lime glass - Conductor: FTO film - Operating frequency: 4.9 GHz - Transparency: 80%	- Measured gain: 5.14 dBi - Demonstrates excellent agreement between measured and simulated results - Offers a directional pattern and stable performance - Ideal for outdoor transparent applications.

TABLE 7. Comparison of other materials used in transparent antenna.

Antenna Type/ References	Structural Characteristics / Design Types	Key Differences and Technical Insights
Water/Ethyl Acetate-Based Patch Antenna [65], [42]	- Substrate: Plexiglass (ε_r = 3.4), Ethyl Acetate (ε_r = 7.8) - Frequency: 1.98 GHz - Circular patch design	- 100% transparency - Liquid substrate allows 48% size reduction compared to air - 35% bandwidth, stable monopolar pattern - Cheap and eco-friendly materials.
Micro-Metal Mesh Conductive MIMO Antenna [38]	- Conductor: Micro-metal mesh - MIMO configuration - Frequency bands: 2.48–2.488 GHz, 5.15–5.8 GHz	- Broadband dual-band operation - Suitable for transparent MIMO systems - Combines mechanical strength with transparency.
Planar Dipole with Ga-Doped ZnO [69]	- Conductor: Ga-doped ZnO- Frequency: 2.4 GHz (ISM band)- Transparent dipole structure	- Gain: 13.97 dBi @ 2.4 GHz - Performance comparable to ITO antennas - Provides a foundation for ZnO-based transparent systems.
High-Frequency Antenna on C-Sapphire [69]	- Substrate: C-Sapphire (ε_r = 9.3)- Frequency: 29 GHz- Conductor unspecified	- Transparency: 90% - Suitable for mmWave applications - High-dielectric substrate supports miniaturization.
Comparison of ITO vs. AgHT-4 on Glass [90]	- Substrate: Pyrex glass- Patch: ITO vs. AgHT-4- Frequency: Not specified	- Gain: 11.5 dBi (ITO), 9.8 dBi (AgHT-4) - ITO on Pyrex gives 92% efficiency - Highlights impact of material pairing.
Transparent UWB Antenna using Conductive Fabric [72]	- Substrate: PDMS- Conductor: Transparent conductive fabric- UWB antenna with flexible design	- Highly flexible & transparent - Maintains functionality under curvature - Suited for wearable and flexible systems.
Water/Ethyl Acetate-Based Patch Antenna [65], [42]	- Substrate: Plexiglass (ε_r = 3.4), Ethyl Acetate (ε_r = 7.8)- Frequency: 1.98 GHz- Circular patch design	- 100% transparency - Liquid substrates allow 48% size reduction compared to air - 35% bandwidth, stable monopolar pattern

substrate. These results reinforce the feasibility of combining TCOs with low-loss, high-frequency substrates to develop high-gain, optically transparent antennas suitable for millimeter-wave applications. Table 4 provides a comparison of different ITO Material-Based Transparent Antenna Designs:

D. COMPOSITE MATERIALS

Composite materials, which integrate various combinations of substrates and conductive layers, have shown significant promise in the development of transparent antennas. A notable example is presented in [61]. where a multilayer thin-film antenna designed specifically for mobile device applications employs a polyimide substrate ($\varepsilon_r = 3.5$) coupled with a copper backing and an IZTO/Ag/IZTO (indium-zinc-tin oxide/silver/indium-zinc-tin oxide) multilayer conductor. The antenna structure features two branches connected by a loop and operate at a center frequency of 2.4 GHz. Fabrication was performed using a DC pulse sputtering technique, and both measured and simulated results

TABLE 8. Summary of transparent reflectarray antennas at mmWave.

Frequency	Antenna Type	Peak gain (dBi)	Gain Bandwidth (%)	Aperture Efficiency (%)	Process	Transmittance (%)
400 GHz [105]	Folded reflectarray Antenna (FRA)	33.66	16 (at 3dBi)	33.65	lithography + PCB	-
20 GHz [106]	Ka-Band High-Efficiency Transparent Reflectarry	27.3	12.9(at 1dBi)	40	prototype with an aperture of 160 x 150 mm2	81
19.3 GHz [107]	Low RCS reflectarray antenna consisting of a feed horn and a SSPP	24.5	11.3 (at 1dBi)	38.7	meshed type SSPP reflector is assembled with 28 dielectric strips	-
26 GHz [108]	Transparent reflectarray using indium tin oxide. 392 elements	22.2	15	-	Quartz wafer	90
14.5 GHz [109]	Quartz glass substrate and ITO as ground	24.1 (pencil) 16.5 (OAM)	-	41.3 (pencil) 6.8 (OAM)	Fine metal line.	82
20 GHz [110]	ITO array, two quartz glass substrate	24.4	20 (at 1.5-dB)	33.3	ITO & glass	75
27.5 GHz [111]	Liquid Crystal and transparent metal mesh	14.35	11	-	photolithography process. GT7 LC dielectric material, Ɛr=3.445	80
30 GHz [112]	Right-handed CP reflectarray	32.5	23.2 (at 3 dBi)	54.9	PET film with FML, quartz, ITO	80.2
28 GHz [113]	CP reflectarray	25.8	17 (at 1.5 dB)	-	ITO & glass substrate	-
25 GHz [114]	An active integrated antenna (AIA) with solar cells	41.3	22.7	-	ITO with soda lime glass. Er=3.68	73.9
11 GHz [115]	16 x16 OTRA , novel via-free magneto-electric	23.0 @10.5 GHz	35.2 (3-dB), 20.6 (1.5-dB)	Peak 44.8	Via-free magneto-electric (ME) dipole using metal mesh (hex + square); single-layer quartz substrate, no air gap	80
30 GHz [116]	32.21 (RHCP), 32.42 (LHCP)	33.7 (RHCP), 30.3 (LHCP)	38.3 (RHCP) and 38.4(LHCP) at 3dBi	32.6 (RHCP), 34.3 (LHCP)	Fine metal lines (FML) patterned on PET/acrylic with ITO backing; ultra-thin (0.1125λ_0	82.8

confirmed reliable performance. The antenna achieved a peak gain of 1.66 dBi and offered key advantages including high transparency (86%), flexibility, and low resistivity, making it suitable for integration into portable and wearable electronics.

Similarly, in [52], the IZTO/Ag/IZTO trilayer conductor was also used with a polyimide substrate under low-frequency operation (1.2 MHz). The configuration yielded comparable results, achieving 1.66 dBi gain and 86% transparency. These findings highlight the value of hybrid multilayer compositions in striking a balance between optical transparency, mechanical flexibility, and RF performance, thereby enabling advanced applications in flexible transparent communication systems.

The following Table 5 highlights the composite material based TRA:

E. FLOURINE-DOPED TIN OXIDE (FTO)

Fluorine-doped tin oxide (FTO) has emerged as a promising TCO material, offering several advantages over conventional alternatives. As reported in [44] FTO demonstrates low

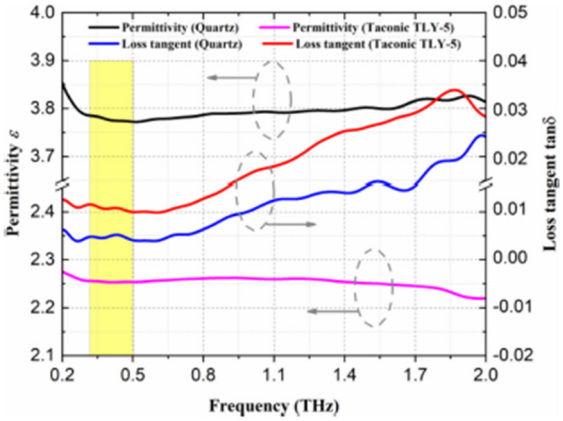

FIGURE 2. Measurements of loss tangent and relative permittivity [101].

TABLE 9. Results of parameters of samples at 400 GHz [101].

Substrate	Thickness (mm)	Di-electric constant	Loss Tangent
Quartz	1.005	3.780	$4.428\text{x}10^{-3}$
	1.006	3.776	$4.445\text{x}10^{-3}$
	1.007	3.773	$4.462\text{x}10^{-3}$
Taconic TLY-5	1.586	2.254	$1.014\text{x}10^{-2}$
	1.587	2.253	$1.014\text{x}10^{-2}$
	1.588	2.252	$1.014\text{x}10^{-2}$

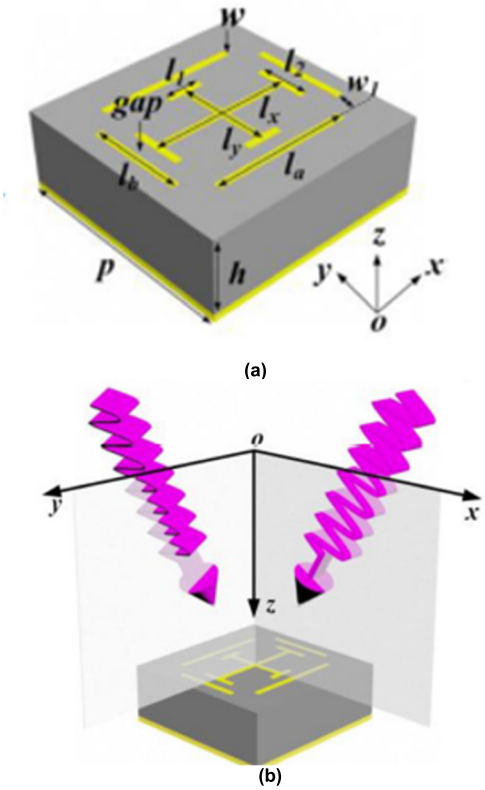

FIGURE 3. (a) Parameters measurement of the proposed element. (b) Definition of the TE and TM source at the excited stage of unit cell by the x-polarized oblique incident plane wave [101].

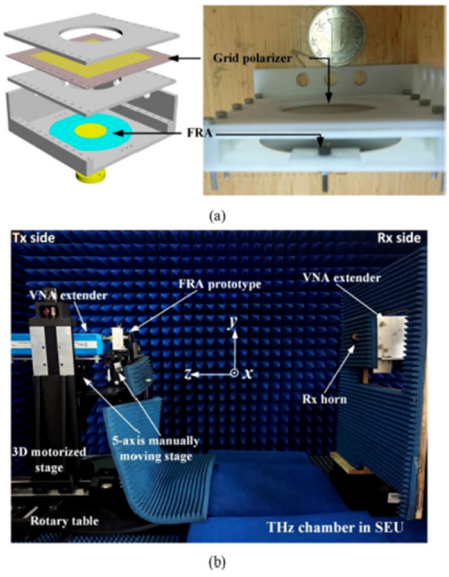

FIGURE 4. (a) FRA antenna. (b) THz measurement at Anechoic chamber [101].

toxicity, a modest plasma frequency, and excellent mechanical, chemical, and thermal stability—making it well-suited for robust antenna designs. The mechanical hardness of SnO2 is approximately 6.5 on the Mohs scale, outperforming ZnO and In2O3, which register around 4 and 5, respectively. FTO also maintains structural integrity in chemically aggressive environments, including prolonged exposure to standing water [81]. In the design of transparent microstrip patch antennas, particularly those integrated with photovoltaic systems, FTO has demonstrated practical viability. As observed in Table 1, FTO used with a Pyrex glass substrate achieved 90% optical transparency at 5 GHz, with a gain of 3.63 dBi. Its superior mechanical durability and environmental resistance make FTO a strong candidate for outdoor applications, as supported by findings in [82], and [83]. Compared to other TCOs such as aluminum-doped zinc oxide (AZO) and indium tin oxide (ITO), FTO exhibits greater resilience and longevity. Additionally, substrates like borosilicate (e.g., Pyrex glass) and quartz, with their low dielectric constants and minimal loss tangents, further enhance the RF performance. Two transparent FTO-based patch antennas fabricated on Pyrex glass have demonstrated resonant behavior in the 2.5–5 GHz range, reinforcing FTO's applicability in transparent and multifunctional antenna systems.

FTO has continued to demonstrate its effectiveness as a transparent conductive material for antenna applications operating across a wide frequency spectrum. In [70] an optically transparent E-shaped patch antenna utilizing FTO with a polyimide substrate was investigated within the 710–785 GHz range. This high-frequency antenna incorporated a Titanium-doped Indium Oxide (TIO) conductive layer, achieving a radiation efficiency of 55% and an

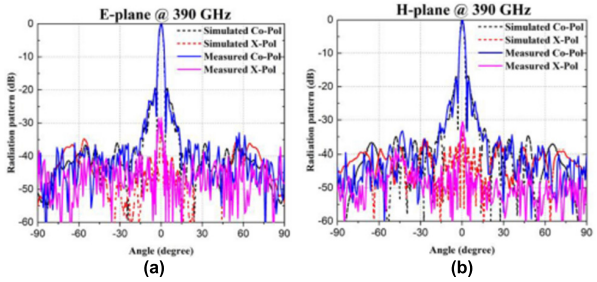

FIGURE 5. Simulated and measured radiatio n patterns of the proposed THz FRA antenna [101].

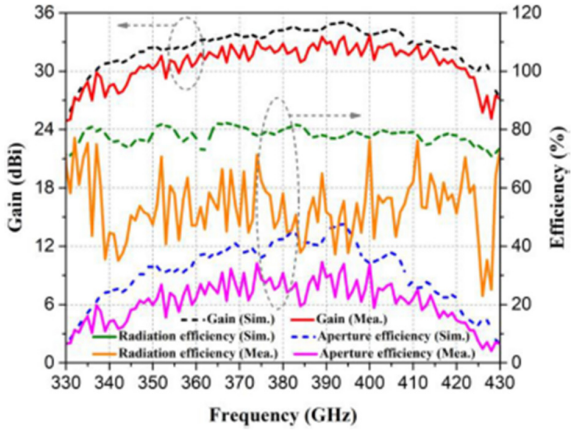

FIGURE 6. Gain and efficiency of the FRA [101].

TABLE 10. Summary of Folded Transparent Reflectarray Antenna (FTRA).

Specific Components Discussed	Structural Characteristics / Design Types	Key Differences and Technical Insights
Reflectarray (RA) Substrate	Fabricated using lithography on quartz	- Enables precise geometry control; quartz chosen for higher permittivity (≈3.78) and lower loss tangent (≈0.0044) vs Taconic TLY-5
Single-layer Phase Element	Orthogonal I-shaped structure with open square ring	- Supports both phase control and polarization conversion, optimizing antenna performance
Grid Polarizer	Thin 0.127 mm PCB-based wire-grid placed in front of RA	- Transparent to RA, reflective to feed; prone to deformation without mechanical support
Support Fixture	3D-printed dual-plate assembly structure for holding the grid polarizer	- Prevents deformation, maintains ray trace accuracy, and ensures consistent radiation performance
Pyramid Horn Feed	Operates from 325–500 GHz with F/D = 1.07	Achieves -10 dB S11 bandwidth; gain of 16.14 dBi at 400 GHz; HPBW: ~27° in both E- and H-plane; edge taper from -11.54 to 9.45 dB
Radiation Patterns	Measured at 390 GHz; evaluated in E- and H-planes	Co-pol shows strong main lobe at 0°, minimal X-pol; measured side lobes and X-pol slightly higher than simulated due to fabrication/measuring errors
Gain and Efficiency	Gain up to 33.66 dBi at 400 GHz; 3-dB gain bandwidth: 357–421 GHz; max aperture efficiency: 34.51% at 389 GHz	Demonstrates high directionality and efficiency for terahertz applications; measured values closely match simulations, validating design

impedance bandwidth of 10%. A peak gain of 3.48 dB was recorded at 730 GHz, with the gain consistently exceeding 2.6 dB throughout the targeted band. At 750 GHz, the antenna exhibited a gain of 3.34 dB, a directivity of 5.58 dB, and radiation efficiency of 59.78%. These performance parameters indicate the antenna's strong potential for next-generation wireless communication systems requiring high gain, wide bandwidth, and directional radiation performance at sub-terahertz frequencies.

Furthermore, FTO has been effectively applied in lower-frequency antenna systems. In [71], a transparent microstrip antenna was fabricated using soda lime glass as the substrate and FTO films as the conductive layers, operating at 4.9 GHz. The antenna achieved a gain of 5.14 dBi and maintained an optical transmittance of 80%, showcasing its ability to maintain both high optical transparency and RF performance. The excellent agreement observed between simulated and measured results confirms the practicality of FTO-based transparent antennas for a variety of emerging applications, particularly where both conductivity and transparency are critical, such as in vehicular displays, smart windows, and integrated photovoltaic-communication systems.

F. OTHER MATERIALS

In the exploration of optically transparent substrates, novel combinations such as distilled water with plexiglass ($\varepsilon_r = 3.4$) and ethyl acetate ($\varepsilon_r = 1.005$) have demonstrated promising results. As reported in [41] and [62] the application of 1.98 GHz frequency resulted in about 100% optical transparency, confirming the feasibility of small water-based patch antennas using liquid substrates with favourable dielectric properties. Ethyl acetate, in particular, serves as an excellent candidate for the central substrate layer due to its high optical transparency, affordability, and elevated permittivity of approximately 7.8 in the microwave frequency range. When employed instead of air, ethyl acetate allows for a 48% reduction in the diameter of the circular patch antenna. Additionally, a wide impedance bandwidth of 35% with a |S11| value below -10 dB, alongside a stable monopolar radiation pattern, was observed, indicating its viability in practical RF applications. Furthermore, micro-metal mesh conductive (MMMC) materials have gained attention for their utility in transparent MIMO antenna design. In [38], both simulation and experimental validation were conducted on a MMMC-based MIMO antenna, showing adequate bandwidth for operation across 2.48–2.488 GHz and 5.15–5.8 GHz frequency bands. Complementarily, silver bus bars have been employed to enhance conductivity while maintaining optical transparency in such designs [84].

The study in [66] presents an optically transparent planar dipole antenna utilizing gallium-doped zinc oxide (GZO),

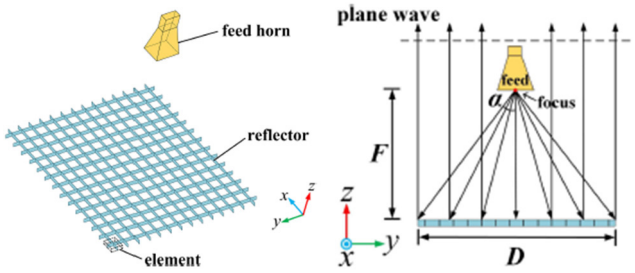

FIGURE 7. Mesh-type low RCS reflectarray antenna and schematic diagram [102].

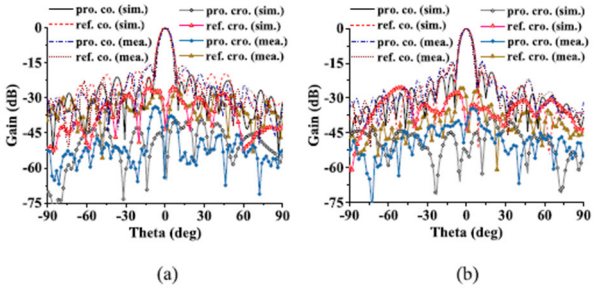

FIGURE 8. Simulated and measured radiation patterns of the proposed low RCS antenna and the reference antenna at 10.0 GHz. (a) E-plane. (b) H-plane [102].

offering performance comparable to traditional ITO-based antennas. Designed for operation at the 2.4 GHz ISM band, the antenna achieved a notable gain of 13.97 dBi, demonstrating the potential of GZO as a viable transparent conductor. Similarly, in [8], a high transparency of 90% was achieved at a higher frequency of 29 GHz using a c-sapphire substrate with a dielectric constant (ε_r) of 9.3, reinforcing the applicability of GZO at mmWave frequencies. As previously discussed, a variety of transparent conducting materials, such as ITO and FTO, have been explored for patch fabrication, while substrates including PDMS, PET, and various forms of glass (quartz, Pyrex, soda-lime, borosilicate) as well as silicon, have been extensively studied. Notably, [85], reports that Pyrex glass substrates combined with ITO patches yielded the highest gain of 11.5 dBi, while AgHT-4 patch material on glass substrates provided a slightly lower gain of 9.8 dBi. Impressively, an efficiency of up to 92% was observed when an ITO patch was paired with a Pyrex glass substrate.

In pursuit of flexible transparent antenna technologies, [69] proposed a novel fabrication method for a flexible UWB antenna using transparent conductive fabric tissue embedded in a PDMS substrate. This antenna preserved its functional integrity across various curvature radii, demonstrating significant mechanical flexibility and robustness. The approach underscores the feasibility of combining transparency with high flexibility, positioning such antennas as strong candidates for future wireless communication systems. The following Table 7 gives a suitable comparison of miscellaneous materials used in transparent antennas:

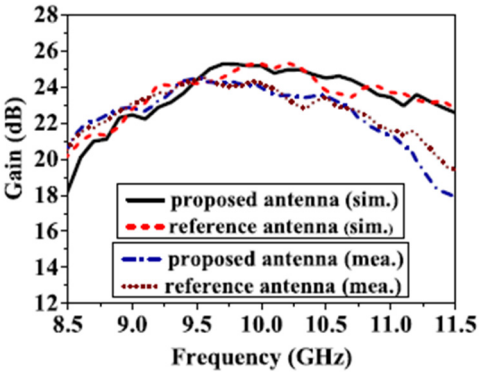

FIGURE 9. Simulated and measured gain of antennas [102].

TABLE 11. Summary of Radar Cross Section Reflectarray Antenna (RCS RA).

Antenna Type Discussed	Structural Characteristics / Design Type	Technical Insights
Mesh-type RCS Reflectarray	- 14 × 14 elements, 238 × 238 mm² mesh-type surface- Transparent in optical band - Uses Spoof Surface Plasmon Polariton (SSPP)-based tunable metallic grating- Linear polarized feed horn at F = 166 mm	- Co- and cross-pol measured at 10.0 GHz- Main lobe at θ = 0°, sidelobes >15 dB below - Cross-pol < –30 dB in E- & H-planes- Gain: 24.5 dBi (meas.) @ 9.6 GHz, 25.2 dBi (sim.) @ 9.7 GHz - Aperture Efficiency: 38.7% (meas.), 44.5% (sim.) - 1-dB Gain Bandwidth: 11.3% (meas.), 12.1% (sim.) (9.2–10.5 GHz / 9.3–10.5 GHz)
Reflector + linear polarized feed horn.	- Similar structure for baseline comparison- No SSPP elements - Traditional solid reflector	- Main beam aligned at 0°, with sidelobe suppression - Gain: ~25.2 dBi (sim.), slightly lower measured - Aperture Efficiency: Not explicitly stated - 1-dB Gain Bandwidth: 13.2% (meas.), 13.9% (sim.) (9.2–10.5 GHz / 9.4–10.8 GHz)

III. TRANSPARENT REFLECTARRAY ANTENNAS IN MILLI-METER WAVE

RA combines the high-gain characteristics of traditional parabolic reflectors with the structural and beam-steering flexibility of flat phased arrays, making them pivotal technology for advanced wireless communication systems [86], [87], [124], and [130]. Their inherent advantages—lightweight construction, cost-effectiveness, ease of fabrication, and the elimination of complex feeding networks—render them

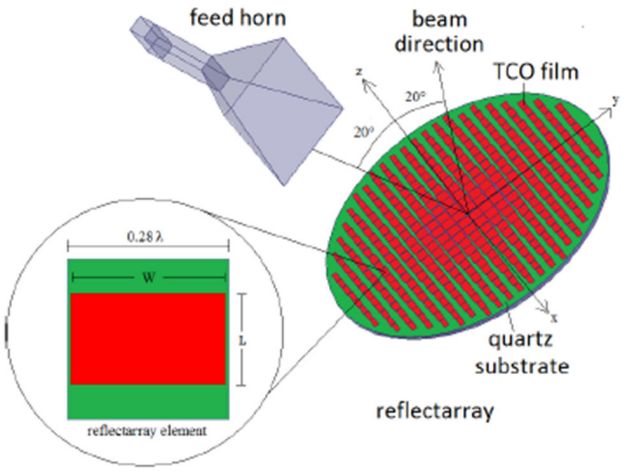

FIGURE 10. Reflectarray design, the red color is conductor [1].

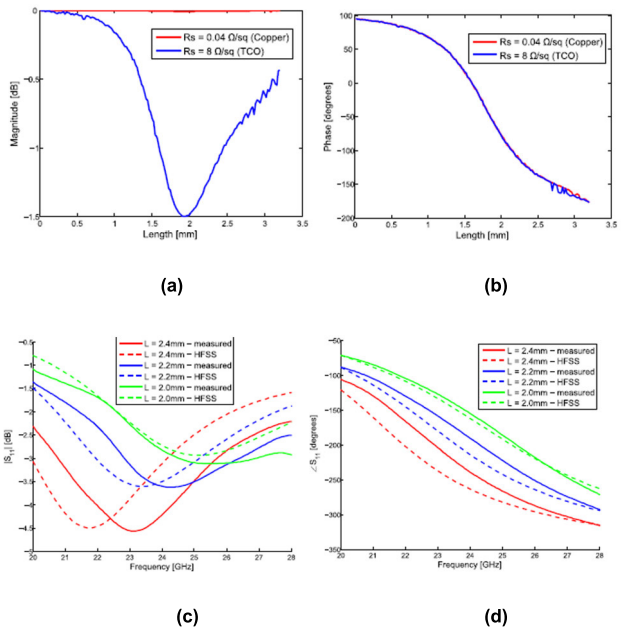

FIGURE 11. Design curves for copper element (a) Magnitude and (b) Phase design curve. (c) Comparison of experimental magnitude and (d) phase curve [1].

highly suitable for applications in satellite communications, radar systems, and long-range point-to-point wireless links [88], [89], [90], [91], and [131].

In parallel, transparent planar antennas have emerged as a compelling innovation due to their multifunctional utility and aesthetic integration capabilities [92], [93]. These antennas can be discreetly deployed on glass surfaces such as building windows or vehicle windshields, where they provide modest communication support while preserving visual clarity. Additionally, their compatibility with photovoltaic surfaces enables co-integration with solar panels, thus optimizing surface area for both energy harvesting and antenna performance [94]. This synergy is particularly beneficial for microsatellites and nanosatellites, where space constraints necessitate multifunctional components. For such platforms, antennas possessing over 90% optical transparency are considered ideal to avoid blocking sunlight needed for power generation [95], [96].

Transparent Reflectarray Antennas (TRAs), which utilize optically transparent conducting materials, most notably ITO—embody the convergence of electromagnetic functionality and optical transparency [97], [98]. These antennas are being increasingly tailored for emerging 5G networks and space-based platforms where their ability to maintain high signal integrity without obstructing visible light is particularly advantageous. However, despite their promise, TRAs still face critical technical challenges, especially related to the inherent conductor loss associated with transparent conductive oxides like ITO [98], [99]. Addressing these limitations remains an active area of research, aimed at enhancing the overall efficiency and viability of transparent antenna technologies for next-generation wireless systems [100].

Table 8 presents a comprehensive comparative analysis of various TRA antenna designs developed for millimeter-wave (mmWave) frequency applications. The surveyed antennas span a broad operational frequency range from 14.5 GHz to 400 GHz, reflecting a growing research interest in merging optical transparency with high-frequency electromagnetic performance for next-generation wireless systems. The comparison emphasizes critical design parameters, including peak gain, gain bandwidth, aperture efficiency, fabrication methods, and optical transmittance, each of which plays a pivotal role in determining the antenna's effectiveness in advanced communication scenarios such as 5G, 6G, and wearable electronics.

A predominant choice of materials across the reported designs includes TCOs such as ITO, alongside substrates like quartz and various types of glass, which offer favorable electromagnetic and optical properties [120], [121]. Notably, an ITO-coated quartz-based antenna operating at 26 GHz demonstrates an impressive 90% optical transmittance, making it a strong candidate for integration into optically exposed environments like smart windows and transparent display systems. Peak gain values among the reported antennas vary widely depending on the design architecture and frequency, with the highest recorded gain of 41.3 dBi achieved by an active integrated antenna (AIA) at 25 GHz. This AIA also incorporates solar energy harvesting, illustrating the viability of multifunctional TRA systems that combine wireless communication with renewable energy integration.

Moreover, several designs adopted circular polarization (CP) to enhance radiation robustness and bandwidth. Among them, CP RA operating at 28 GHz and 30 GHz exhibit peak gains of 25.8 dBi and 32.5 dBi, respectively. The latter also demonstrates superior performance with a broad gain bandwidth of 23.2% and an aperture efficiency reaching 54.9%, the highest among the surveyed entries. These results affirm the capability of TRA to deliver competitive mmWave

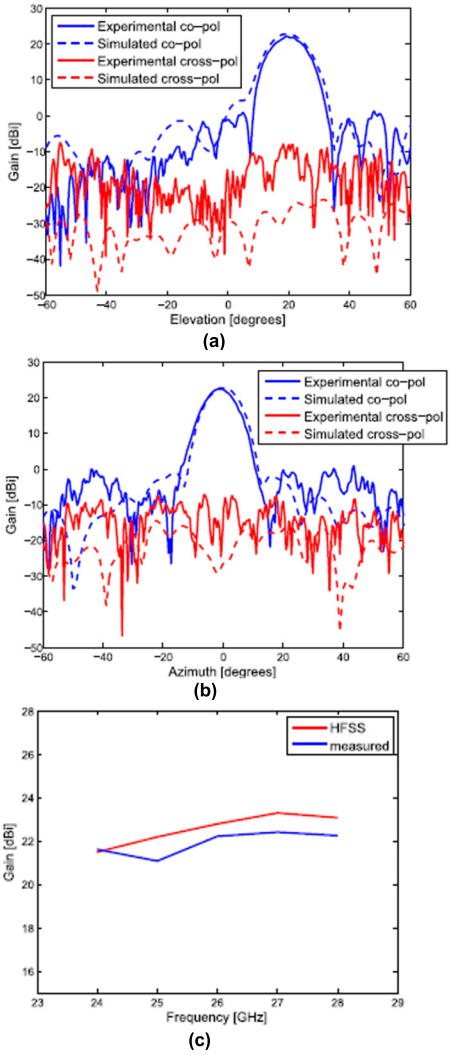

FIGURE 12. Simulated (Rs = 8 Ω/sq) and experimental far-field patterns. (a) Vertical cut. (b) Horizontal cut at 20° elevation [8]. (c) Simulated (HFSS) and measured bandwidth comparisons [1].

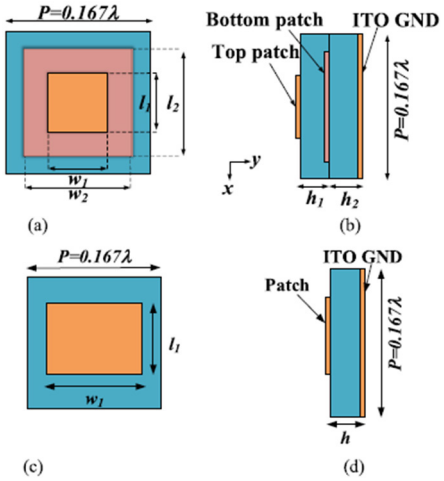

FIGURE 13. (a) Front and (b) side view of the double-layer patch of a proposed element. (c) Front and (d) side view of the single- layer patch. Note: Blue parts are glass substrates and orange patches are of ITO films [25].

performance while offering additional advantages in terms of aesthetic and multifunctional integration.

The bandwidth performance across the reported TRA designs, as summarized in Table 8, ranges from 11% to 23.2%, reflecting sufficient wideband characteristics suitable for mmWave applications. These bandwidth levels are adequate to support high data-rate wireless communication systems, making the designs viable for modern 5G and emerging 6G technologies. The employment of advanced fabrication techniques—such as photolithography, the implementation of fine metal lines, and the use of PET films—demonstrates the continual effort to optimize the trade-offs between optical transparency, structural complexity, and RF performance.

Optical transmittance among these antennas generally exceeds 70%, with several designs surpassing 80%, underscoring their strong applicability in environments that demand both high electromagnetic performance and aesthetic or functional transparency. Such transparency is particularly crucial in systems where antennas must remain visually unobtrusive, such as in transparent displays, smart windows, and solar-integrated devices.

Collectively, the antenna configurations presented in Table 7 signify a rapidly advancing domain of TRA technology. The ability to achieve high gain, acceptable aperture efficiency, and broad bandwidth, without sacrificing optical transparency, positions these antennas as strong candidates for integration into smart infrastructure. They hold significant promises for a range of applications, including vehicular communications through transparent windows, augmented reality (AR) systems, wearable electronics, and energy-harvesting platforms—where multifunctionality and seamless visual integration are paramount.

Further explanation is provided in the following by referring to each antenna in context of Table 8.

A. FOLDED TRANSPARENT REFLECTARRAY ANTENNA

As summarized in Table 9, the work presented in [100] and [129] introduces several innovative methodologies in the development of a 400-GHz Folded Transparent Reflectarray (FTRA) antenna, specifically designed for terahertz (THz) applications. This design emphasizes compactness, transparency, and performance enhancement at submillimeter-wave frequencies. A notable fabrication approach includes the use of lithography on a quartz substrate, which facilitates the precise patterning of high-frequency components while maintaining optical transparency. The antenna employs a single-layer RA structure, thereby minimizing thickness and enabling integration into compact and planar platforms. This FTRA design highlights the expanding possibilities in transparent and high-frequency antenna technology, especially in the context of compact, multifunctional systems envisioned for 6G and beyond. The methods adopted here set a benchmark for future research targeting the integration of optical

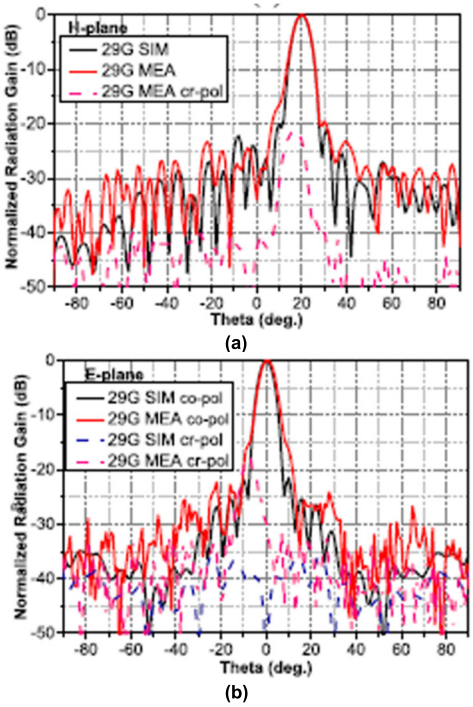

FIGURE 14. Simulated and measured radiation patterns at 29 GHz (a) H-plane and (b) E-plane [25].

TABLE 12. Summary of Indium Tin Oxide Reflectarray Antennas (ITO RAs).

Antenna Type Discussed	Structural Characteristics / Design Type	Technical Insights
26 GHz Quartz-based ITO RA (392 elements	- Rectangular patch on 1 mm quartz (εr = 3.8) - Periodicity: 0.28λ (3.23 mm) - Beam: 20° off-broadside via offset WR-42 horn - Subwavelength hybrid patch design	- Simulated gain: 22.9 dBi - Measured gain: 22.2 dBi - Phase range: 272° (essential for low-error beam steering) - Bandwidth: >15%, limited >28 GHz by measurement setup - X-Pol isolation: ~40 dB below peak
28 GHz ITO RA (2916 elements, 9λ × 9λ aperture)	- Larger aperture with F/D = 0.7 for optimal incidence distribution - Surface resistance model: 8 Ω/sq for ITO - Subwavelength hybrid geometry maintained	- Measured peak gain: 25.8 dBi at 28 GHz- Simulated patterns closely match experimental- Sidelobe levels: – 22.9 dB (H-plane), –24.1 dB (E-plane) - X-Pol: up to –60 dB in H-plane- Bandwidth: 26–30 GHz

transparency and terahertz functionality in next-generation wireless communication platforms. Here are the key methodologies highlighted:

- *Use of Lithography on Quartz*: The antenna utilizes a single-layer RA structure, fabricated through a lithography process on a quartz substrate. This fabrication approach enables precise geometric definition of the unit cells, which is critical for tailoring the electromagnetic response and achieving the desired phase distribution at terahertz frequencies.

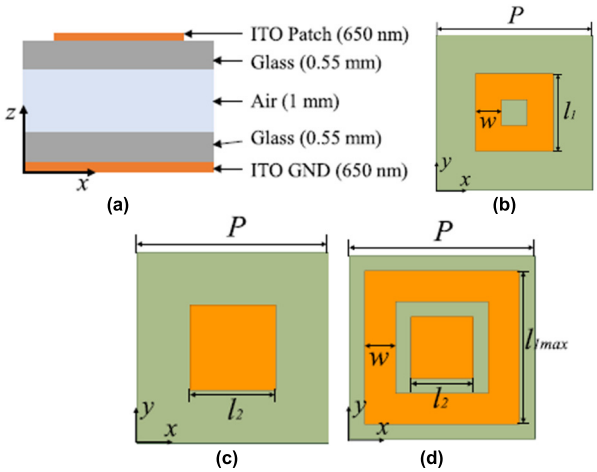

FIGURE 15. (a) Multilayer hybrid dielectric (b) Square ring. (b) Square patch. (c) Square ring and square patch together [21].

- *THz Time-Domain Spectrometer System*: To ensure precise antenna design, the researchers employed a terahertz (THz) time-domain spectrometer to characterize the electromagnetic properties of the supporting dielectric materials. This method provides accurate permittivity and loss tangent data at THz frequencies, facilitating the integration of realistic material parameters into the simulation and fabrication process.
- *Design of a Single-Layered Phase Element:* The study introduces a novel single-layer phasing element configuration consisting of orthogonally arranged I-shaped structures integrated with an open square ring. This innovative geometry facilitates simultaneous phase modulation and polarization conversion, both of which are essential for enhancing the performance and functional versatility of the RA.
- *Integration of a Wire-Grid Polarizer*: A wire-grid polarizer, fabricated using PCB technology, is strategically positioned in front of the RA and terahertz (THz) feed. This polarizer is engineered to exhibit high transparency toward the reflected RA signal while effectively reflecting the direct feed signal. Such selective transmission and reflection enhance the overall efficiency and performance of the antenna system by optimizing energy redirection and minimizing losses.
- *3-D Printed Fixture for Assembly*: The assembly of the antenna components is achieved using a 3D-printed fixture, which provides a precise and stable platform for aligning and securing the individual elements. This fabrication technique ensures accurate spatial configuration of the RA and feed system, which is essential for maintaining optimal electromagnetic performance, particularly at terahertz frequencies where minor misalignments can lead to significant performance degradation.

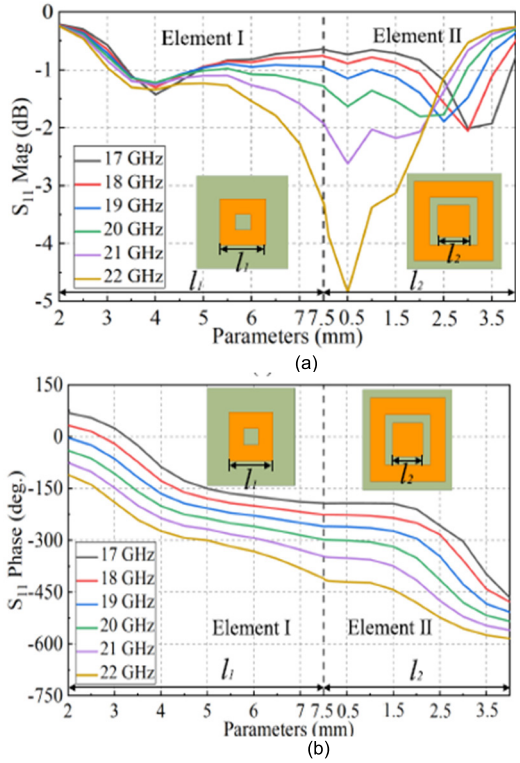

FIGURE 16. Simulated (a) magnitude and (b) phase responses of the designed heterogeneous ITO elements [21].

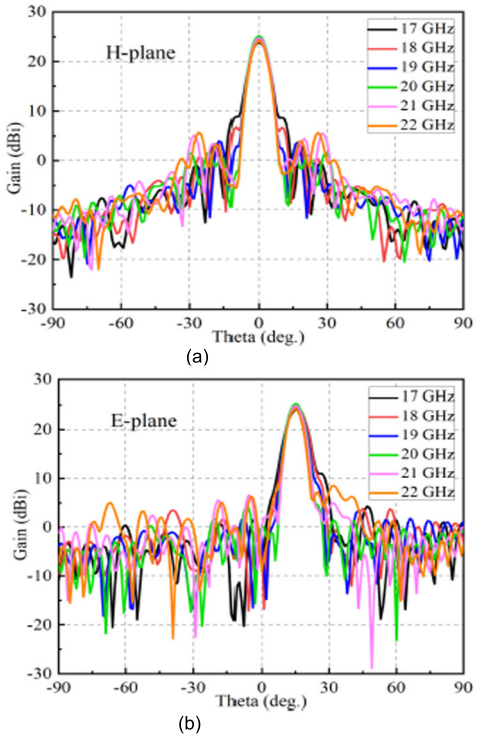

FIGURE 17. Simulated radiation patterns of RA (a) H-plane and (b) E-plane [21].

- *Experimental Validation of Performance*: This paper presents the experimental validation of the antenna's performance, demonstrating a peak gain of 33.66 dBi at 400 GHz and a 3-dB gain bandwidth of 16%, covering the frequency range from 357 to 421 GHz. This empirical analysis substantiates the accuracy of the theoretical design while offering valuable insights into the practical challenges encountered during fabrication, assembly, and high-frequency performance evaluation.

These methodologies collectively contribute to the advancement of high-gain antennas in terahertz applications [100], [101], representing a synergistic integration of innovative design concepts, precise fabrication techniques, and comprehensive experimental validation.

Figure 2 presents a comparative analysis of the dielectric properties—specifically, permittivity (ε) and loss tangent (tan δ)—of Quartz and Taconic TLY-5 substrates across the 0.2 to 2.0 THz frequency range. Quartz demonstrates consistently higher permittivity, maintaining a value close to 3.8, while Taconic TLY-5 exhibits a lower permittivity, gradually increasing from approximately 2.2 to 2.5 as frequency increases. In terms of dielectric losses, Quartz maintains a significantly lower loss tangent (ranging from ∼0.003 to 0.006), indicating superior low-loss performance. Conversely, Taconic TLY-5 shows a rising loss tangent trend from ∼0.008 to 0.03, reflecting higher energy dissipation at increasing frequencies. The highlighted frequency window (0.2–0.5 THz) in yellow denotes a region where both substrates maintain relatively stable permittivity and manageable dielectric losses, suggesting their potential applicability in specific terahertz antenna systems. Overall, Quartz, with its superior dielectric stability and low loss, emerges as a more favourable choice for high-performance terahertz antenna designs. On the other hand, Taconic TLY-5 may be considered for scenarios where flexibility in substrate selection is permitted by design constraints.

Furthermore, Table 9 summarizes the detailed geometrical parameters of the proposed 400 GHz FTRA, while Figure 3 visually illustrates the structural layout, offering a comprehensive perspective of the design framework.

The frequency range highlighted in yellow (0.2–0.5 THz) represents a region where both Quartz and Taconic TLY-5 substrates show steady permittivity and acceptable levels of dielectric loss. This indicates that both materials could be useful for certain terahertz antenna applications. Quartz, due to its stable permittivity and lower loss tangent, is more suitable for high-performance and low-loss antenna designs. In contrast, Taconic TLY-5 may be appropriate in situations where more flexibility in material choice is needed, depending on design requirements.

In addition, Table 9 provides detailed information on the dimensions and key specifications of the 400 GHz FTRA

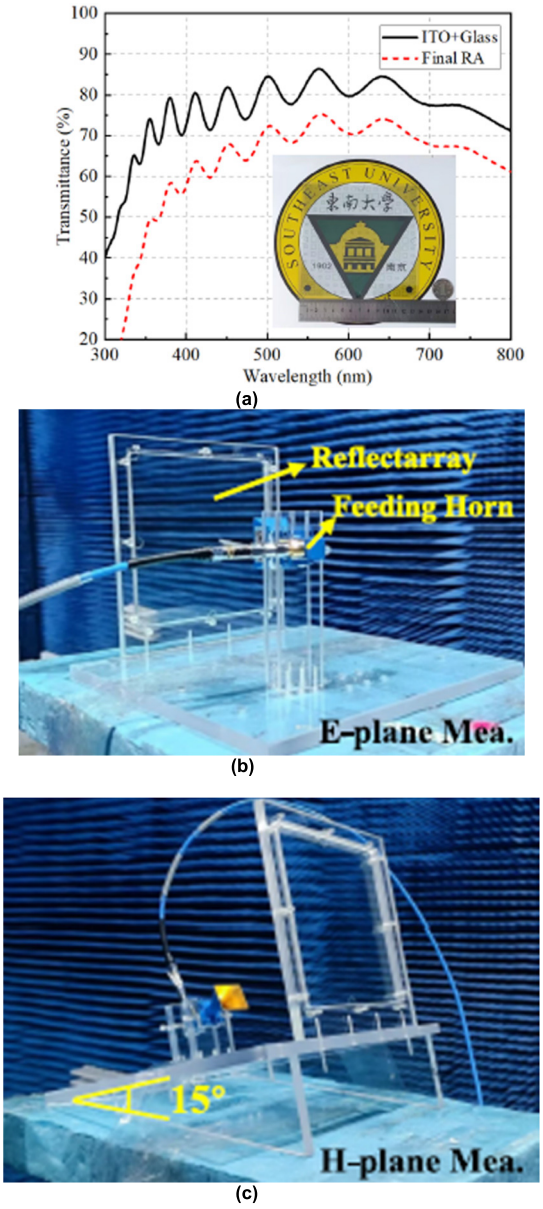

FIGURE 18. (a) The fabricated ITO optically transparent reflectarray and measurement results and (b) Experimental setup [21].

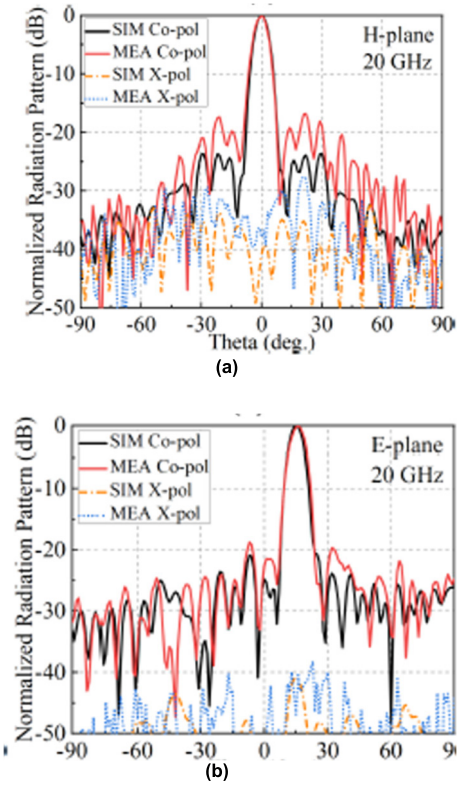

FIGURE 19. Simulated and measured radiation patterns at 20 GHz (a) E-plane and (b) H-plane [21].

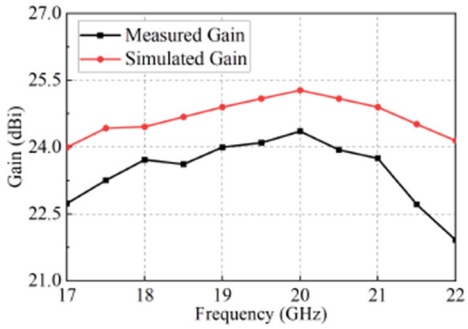

FIGURE 20. Simulated and measured gain results [21].

antenna. Figure 3 shows the antenna's structure, giving a clear understanding of its physical layout and design features.

Figure 6 presents the gain characteristics of the proposed terahertz FTRA. The antenna demonstrates a 3-dB gain bandwidth ranging from 357 GHz to 421 GHz, with the maximum gain recorded at 33.66 dBi at 400 GHz. Additionally, the highest aperture efficiency achieved is 34.51%, observed at 389 GHz, indicating the design's effectiveness at terahertz frequencies.

Table 10 provides a summary of FTRA's design features and technical performance. It outlines key structural components, phase-tuning elements, fabrication techniques, and performance metrics, offering a comparative view of how each element contributes to the antenna's overall efficiency and operational bandwidth.

B. RADAR CROSS SECTION REFLECTARRAY ANTENNA

Radar Cross Section (RCS) reduction techniques in RA aim to reduce the antenna's detectability by radar systems while ensuring reliable communication performance [108], [109], [110], [123]. Recent developments in this domain have explored innovative structural designs and novel materials to improve antenna efficiency across different frequency ranges.

As summarized in Table 2, the antenna proposed in [102] demonstrates high performance with an aperture efficiency of 44.5% and a peak gain of 25.2 dBi. It also offers a 1-dB gain bandwidth of 13.9%, operating effectively between 9.4 and

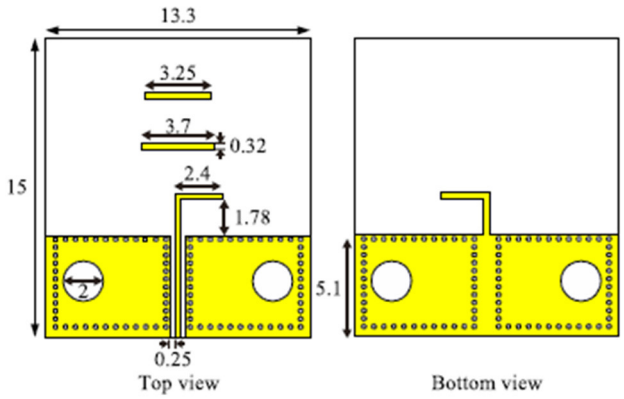

FIGURE 21. Geometry of Active integrated antenna (unit: mm) [105].

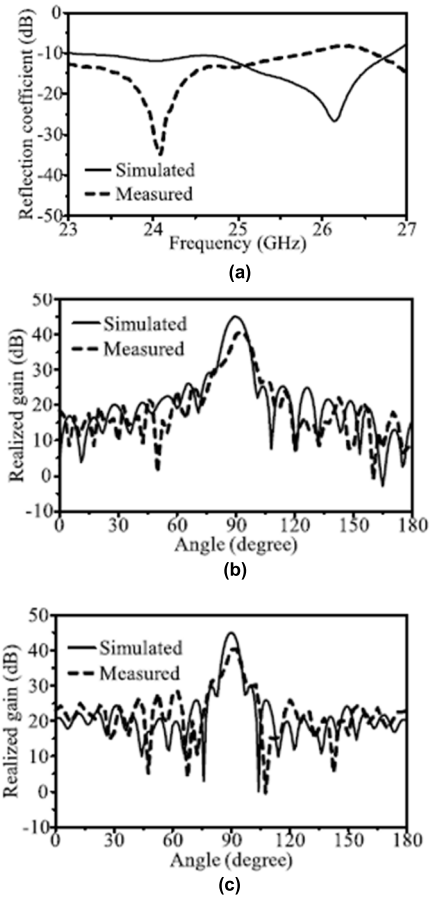

FIGURE 22. (a) Reflection coefficients. (b) Gain Patterns at E-plane. (c) H Plane [105].

10.8 GHz. These parameters show notable enhancements over several existing designs and can serve as a reference point for future research in this area.

A significant contribution from [102] includes the introduction of a mesh-type RA based on spoof surface plasmon polariton (SSPP) technology. This design successfully balances low RCS with high radiation efficiency, an essential feature for stealth and radar-avoidance applications. By adjusting the length of metallic grating structures, the reflection phase of each unit cell can be finely tuned. This adjustability facilitates effective transformation of spherical waves into planar waves, enabling precise beam control. The integration of SSPP structures thus marks a meaningful progression in the development of advanced, low-RCS RA.

The antenna configuration consists of a TRA surface and a feed horn, as illustrated in Figure 7. The reflector comprises a 14×14 array of unit elements, offering optical transparency in the visible spectrum. A linearly polarized horn antenna is employed as the feed source for the RA. The focal distance between the feed and the spoof surface plasmon polariton (SSPP)-based reflector is specified as $F = 166.0$ mm.

The horn antenna is center-fed and features a half-power beamwidth denoted by α, ensuring focused illumination of the array. The total physical dimensions of the mesh-type reflector measure 238.0 mm $\times$ 238.0 mm, corresponding to the 14-by-14 grid of unit cells. This geometric arrangement is critical in maintaining precise phase control and contributing to the overall gain and beam-shaping capabilities of the antenna system.

The performance of the fabricated antennas was evaluated in a microwave anechoic chamber to ensure accurate radiation pattern measurements. Figures 8(a) and 7(b) illustrate the co-polarization and cross-polarization radiation patterns for both the reference and proposed antennas. According to the simulated results at 10.0 GHz, the main lobe in both the E-plane and H-plane is centered at $\theta = 0°$, indicating effective beam alignment.

Additionally, the first sidelobe levels in each pattern are suppressed by more than 15 dB relative to the main lobe, demonstrating good directional performance. Notably, the proposed antenna exhibits excellent polarization purity, with cross-polarization levels below -30 dB in both the E- and H-planes. These results confirm that the antenna maintains low unwanted polarization and exhibits well-defined radiation characteristics, making it suitable for applications requiring high radiation efficiency and minimal interference.

As illustrated in Figure 9, the proposed antenna demonstrates strong performance metrics, achieving a maximum measured gain of 24.5 dBi at 9.6 GHz and a simulated peak gain of 25.2 dBi at 9.7 GHz. The measured aperture efficiency peaks at 38.7%, while the simulated efficiency reaches up to 44.5%. These results indicate that the mesh-type reflector integrated into the design successfully reflects a substantial portion of the incident energy within the target frequency band, thus enabling gain performance comparable to that of the reference antenna.

The measured 1-dB gain bandwidths are 13.2% and 11.3%, corresponding to frequency spans of 9.2–10.5 GHz. In simulation, the reference antenna achieves a 1-dB bandwidth of 13.9% (9.4–10.8 GHz), while the proposed design yields 12.1% (9.3–10.5 GHz). These findings highlight the design's robustness and reliability, making it well-suited for applica-

TABLE 13. Comparison of multilayer ITO-Based RA designs.

Antenna Type/References	Structural Characteristics / Design Type	Key Differences / Technical Insights
ITO-based Optically Transparent RA	- Multilayer hybrid substrate using ITO layers on two quartz glass plates separated by an air gap- 15 × 15 elements, F/D = 0.9- Element I (square patch) and Element II (square ring)- Use of heterogeneous resonance elements	- Achieved 494° phase range at 20 GHz - Reflection loss < 1.8 dB - Simulated gain: 25.3 dBi, Measured: 24.4 dBi- 75% optical transparency, 20% gain bandwidth at 1.5 dB - Effective beam steering with low squinting < 0.5°
ITO-based RA with Soda-Lime Glass	- Two-layer unit cell separated by 0.01 mm air spacer - Substrate: Soda-lime glass (ε_r = 7.2, tanδ = 0.02), thickness: 0.7 mm - ITO thickness: 1.2 µm (σ = 2.4 × 10^5 S/m)	- Adds stealth/RCS reduction functionality - Combines electromagnetic control and wave absorption - Focused on multifunctionality beyond gain or transparency
Transparent RA with AIA for CubeSat	- ITO-based TRA integrated with Active Integrated Antenna (AIA)- Substrate: Soda-lime glass- Transparent RA used on solar panels- Operates at 25.0 GHz	- Realized gain: 41.3 dB with AIA - Combines microwave power amplification and solar energy harvesting - Antenna area: 110 × 80 mm² - Dual-purpose structure: communication + energy harvesting - Enables integration on space-constrained CubeSat surfaces

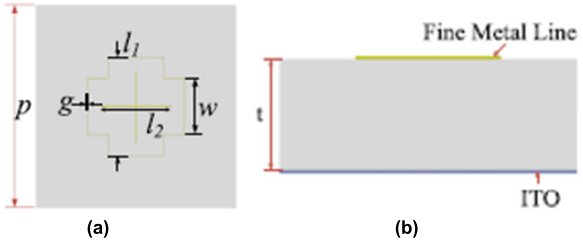

FIGURE 23. (a) Perspective Reflectarray Top view. (b) Side view [103].

tions that require both high gain and moderate broadband capabilities in the X-band frequency range.

C. USING INDIUM TIN OXIDE

Significant research efforts have focused on optically transparent planar antennas based on TCOs, particularly for integration with solar panels [111], [112]. Despite this interest, high conductor losses inherent to TCO materials pose a major challenge in antenna design. The study presented in [1] as summarized in Table 3, addresses this issue by aiming to develop a fully transparent RA using ITO, a widely used TCO. To mitigate the adverse effects of conductor loss, the

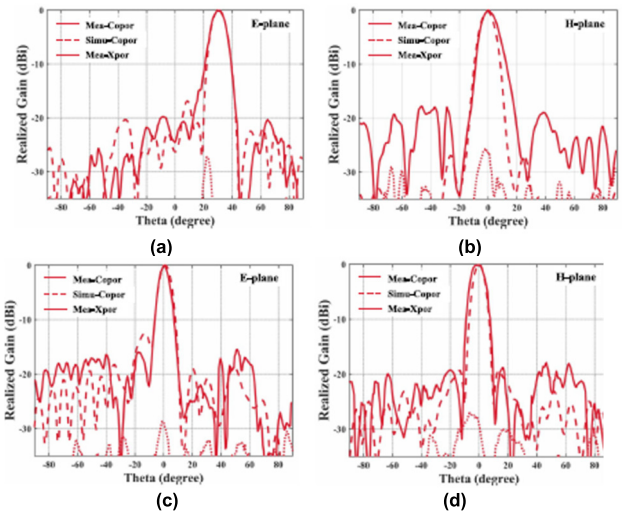

FIGURE 24. Measured radiation patterns of normal feed RA. (a) 13.5G at E-plane. (b) 13.5G at H-plane. (c) 12.5G at E-plane. (d) 12.5G at H-plane [103].

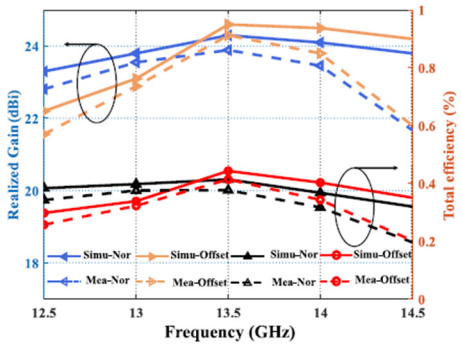

FIGURE 25. Simulated and measured gain [103].

design incorporates subwavelength rectangular patch elements capable of achieving a 272° phase range.

Various techniques are explored in [1] to improve performance, including the use of different patch geometries and subwavelength configurations, all intended to reduce the impact of loss in TCO-based RA designs. Additionally, the study evaluates the electromagnetic behavior of lossy unit cells through both simulations and experimental measurements. A complete RA prototype operating at 26 GHz is successfully fabricated and tested, demonstrating a strong agreement between the simulated results and experimental data. This validates the proposed approach and offers a promising path for future developments in TRA technology.

Figure 10 illustrates the configuration of the proposed RA element. The design features a rectangular patch fabricated on a 1 mm thick quartz substrate, which has a $_r$ of 3.8. Each unit cell is arranged in a square lattice with a periodicity of P = 0.28λ (approx. 3.23 mm), optimized for operation at 26 GHz. To ensure appropriate spacing between adjacent elements, the patch width is limited to a maximum of 3.1 mm. The phase response of the reflected wave, which is essential

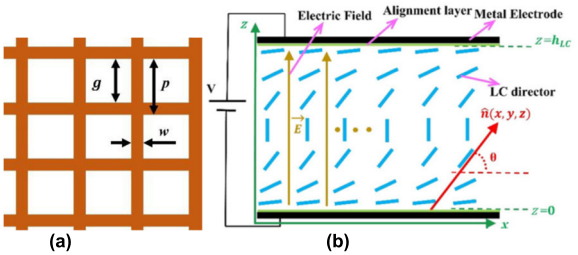

FIGURE 26. (a) Metal mesh structure and design parameters. (b) an LC layer for antenna [100].

for beam control, is regulated by adjusting the cell length (L), given that the incident wave is vertically polarized.

The complete TRA comprises 392 elements arranged in a circular aperture with a 3-inch diameter. It adopts an offset parabolic profile with a focal length of 8.0 cm. The beam is steered 20° off the broadside direction, corresponding with the feed alignment achieved using a WR-42 pyramidal horn antenna placed at a 20° offset in the E-plane. This configuration demonstrates effective beam steering and efficient use of transparent materials for high-frequency RA applications.

Figure 11(a) and (b) present the phase response characteristics of RA elements designed with surface resistances of 0.04 Ω/sq (representing copper) and 8 Ω/sq (representing transparent conductive oxide, TCO), both with a periodicity of 0.28λ. The analysis of patch element lengths reveals that a maximum phase variation of 272° is achievable. It is observed that reducing the unit cell periodicity results in a narrower phase range, which is undesirable, as maintaining a phase range of at least 270° is essential for minimizing phase quantization errors and achieving efficient beamforming in RA designs.

Figure 11(c) compares the reflection coefficients obtained from both simulation and measurement. When applying a surface resistance of 8 Ω/sq in the model, the peak reflection losses from the experimental results closely match the simulated values, confirming the accuracy of the design. Moreover, the smooth slope of the phase response curves suggests that the element design is robust against fabrication-induced deviations, introducing minimal phase error. These findings validate the reliability of the proposed unit cells and support their suitability for practical RA implementations.

The simulation results indicate strong co-polarization to cross-polarization isolation, with cross-polarization levels remaining approximately 40 dB below the peak gain. The theoretical aperture gain of the final RA was calculated to be 25.8 dBi, which aligns well with the observed data and suggests that the system experiences approximately 3 dB of loss. As shown in Figure 12(c), the measured maximum gain of the fabricated RA is 22.2 dBi—very close to the expected value of 22.9 dBi listed in Table 8. This confirms that, despite the inherent losses associated with ITO thin film, high efficiency and effective RA performance can still be achieved through careful design and implementation.

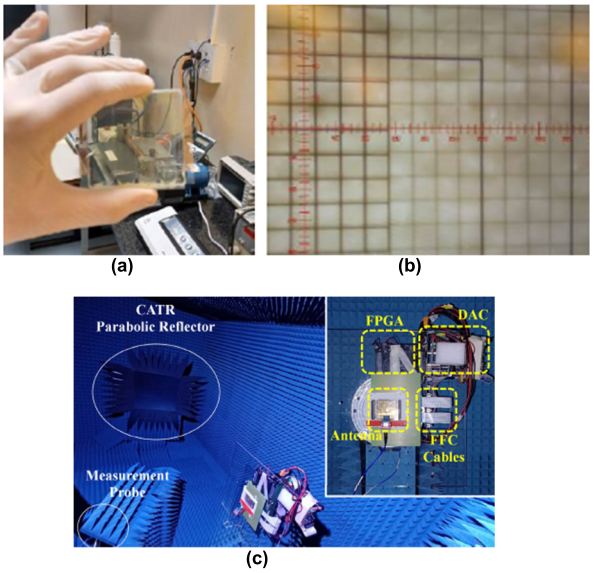

FIGURE 27. Fully assembled prototype with fiber optic spacers. (a) RA sample, filled with GT7 LC. (b) Two-layer zoomed-in view demonstrating two metal mesh layers' alignment (c) measurement setup in an anechoic chamber [100].

Additionally, the bandwidth exceeds 15%, although the gain response at 26 GHz is not symmetric, indicating some asymmetry in radiation behavior. Measurement limitations prevented reliable data collection above 28 GHz; however, the results suggest that the RA design has the potential to support significantly wider bandwidths under improved testing conditions.

In a related study, ITO was employed to fabricate a RA with an aperture size of 9λ× 9λ, where λ corresponds to the wavelength at 28 GHz. The design consists of a 54 × 54 element array, as illustrated in Figure 14. This configuration was developed to demonstrate the feasibility of constructing ITO-based RAs that maintain high radiation efficiency. The successful implementation of such a dense element array using a transparent conductive material like ITO underscores its potential for advanced, low-profile antenna applications, particularly in scenarios where optical transparency and efficient electromagnetic performance are simultaneously required.

An optimal trade-off between beam quality and mechanical configuration is achieved by selecting an F/D of 0.7. Once the horn's offset angle, the F/D ratio, and the RA aperture dimensions are established, the incident field distribution across the RA aperture can be readily determined.

Comprehensive measurements of the complete ITO-based RA antenna were conducted in a far-field anechoic chamber. As illustrated in Figure 14, the RA's primary beam is naturally steered 20° off-broadside, with a measured peak gain of 25.8 dBi at 28 GHz—closely matching the simulated value. In the H-plane, the first sidelobe levels are suppressed by 22.9 dB relative to the main lobe, while in the E-plane, sidelobe suppression reaches 24.1 dB. Figure 14 also com-

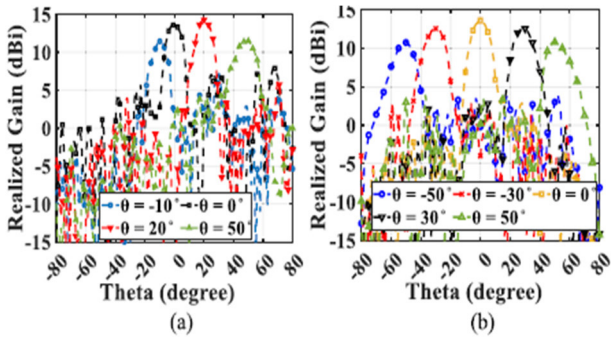

FIGURE 28. Measured beam-steering radiation pattern for (a) $\phi = 90°$ E-plane and (b) $\phi = 0°$ H-plane at the center frequency (f = 27.5 GHz) [100].

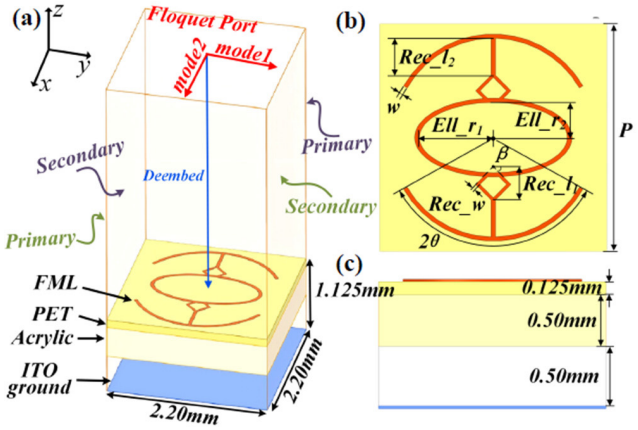

FIGURE 29. (a) Schematic diagram of optically transparent RA cell, (b) top view, (c) side view. P = 2.2, Rec_l1 = 0.34mm, Rec_l2 = 0.37mm, Ell_r1= 0.76mm, Ell_r2 = 0.38mm, w = 0.04mm, Rec_w = 0.03mm, $\beta = 45°$, $\theta = 60°$ [107].

pares the normalized co-polarized and cross-polarized radiation patterns across the 26–30 GHz operational frequency band. The maximum cross-polarization level in the H-plane remains over 60 dB below the main lobe direction, confirming excellent polarization purity.

The use of novel sub-wavelength hybrid patch elements contributes to the improved bandwidth performance of the proposed ITO RA, making it superior to many conventional RAs. Despite ITO's lower electrical conductivity compared to metals like copper, the results demonstrate that a well-optimized ITO-based RA can still achieve high radiation efficiency. A summary of key design features and performance metrics for ITO-based RA antennas is presented in Table 12.

D. USING MULTILAYER HYBRID SUBSTRATE

An optically TRA antenna based on ITO is presented in [21], showcasing a multilayer structure that enhances both electromagnetic and optical performance. The antenna comprises an ITO ground plane, a patterned ITO array, and two quartz glass substrates separated by an air gap. This air gap serves to reduce the high conductor losses typically associated with ITO, thereby improving the overall radiation efficiency. By incorporating a combination of single- and dual-resonant unit cell designs, the RA achieves an extended phase variation, with a measured 494° phase shift at the center frequency of 20 GHz and a reflection loss of less than 1.8 dB.

To validate the design, a 15 × 15-element RA prototype with a F/D ratio of 0.9 was fabricated, simulated, and experimentally tested. The structure demonstrates high optical transmittance of 75%, a 20% gain bandwidth within 1.5 dB variation, and a peak measured gain of 24.4 dBi. The performance results indicate excellent radiation characteristics and a favorable balance between electromagnetic and optical transparency. Compared to earlier ITO-based TRA, this design offers superior phase control, low return loss, wide bandwidth, and high transmission in the visible range, making it highly promising for applications requiring both transparency and efficient radiation.

Excessive glass thickness in RA designs can undesirably increase the overall profile of the antenna and stimulate surface waves on the microstrip layer, potentially degrading performance. To address these limitations, incorporating an air layer within the dielectric substrate offers a practical solution. This modification effectively reduces the substrate's dielectric constant, thereby mitigating conductor losses. Additionally, employing a thick substrate with a low dielectric constant can enhance the operational bandwidth of RA elements, which is critical for high-performance applications. As illustrated in Figure 15(a), proposed multilayer hybrid dielectric architecture, combining layers of glass and air, is introduced to realize these advantages.

The impact of element geometry on phase performance is highlighted in Figures 15(b) and 15(c). The square ring element (Figure 15b) achieves a phase variation of 259° with a higher maximum reflection loss of approximately 1.3 dB. In contrast, the square patch element (Figure 15c) demonstrates a smaller phase range of 176° but with a lower reflection loss of around 0.6 dB. These results emphasize the trade-offs between phase tuning capability and reflection efficiency, guiding the selection of unit cell geometries based on application-specific performance requirements.

Figure 16 illustrates the return loss and corresponding phase shift behavior of the proposed RA elements. Element I independently achieves a phase shift range of 259°, while Element II contributes an additional 235°, both measured at the center frequency of 20 GHz. When these two element types are combined in a hybrid configuration, the overall phase shift range is significantly extended to 494°, enabling enhanced beamforming capabilities. Notably, this wide phase coverage is attained while maintaining a return loss below 1.8 dB, indicating efficient impedance matching and minimal signal reflection. This design approach confirms that combining heterogeneous resonance elements can effectively overcome the limitations of individual geometries and yield wide phase tunability essential for high-performance RA systems.

Figure 17 presents the simulated radiation patterns of the designed ITO-based RA. At 20 GHz, the RA exhibits a peak

TABLE 14. Comparison of transparent Reflectarray Antennas using Fine Metal Line (FML) and Related Structures.

Antenna Type/References	Structural Characteristics / Design Type	Key Differences and Remarks
FML-Based Reflectarray[[110]	- Quartz glass substrate - Transparent ITO ground plane - Fine metal line (FML) pattern with metal cross and folded square ring - Linewidth ≤ 50 µm	- Achieves high optical transparency (82%) - Offers 360° phase variation from 12.5–14.5 GHz - Realized gain: 24.3 dBi (offset feed) - High efficiency (41.3%) and low return loss (2.8 dB)
Folding Reflectarray with Metasurfaces and FSR [110]	- Dual-layer metasurface - Incorporates frequency selective rasorber (FSR) and polarization-conversion metasurface - Designed for RCS reduction	- Adds stealth/RCS reduction functionality - Combines electromagnetic control and wave absorption - Focused on multifunctionality beyond gain or transparency
LC + FML + Transparent Mesh RA[112]	- 10×10 patch array - Transparent metal mesh ground - GT7 liquid crystal cavity - Voltage-controlled beam steering	- Dynamic beam-steering with 260° phase shift - Optical tint (milky-yellow) due to UV exposure of LC - Realized gain: 14.35 dBi at 27.5 GHz - Beam scan range: ±50° (H-plane), up to -50° (E-plane)
Transparent Metal Mesh Only [112]	- Copper mesh with 1.2 µm thickness - Glass substrate with 2 metal-coated layers - Rs = 0.11 Ω/sq, T = 87.1%	- Focused on maximizing optical transmittance - No dynamic tuning (fixed-beam) - Supports EM conduction while allowing visible light transmission.
AIS Dual-CP FML [117]	AIS-based structure with copper FML on PET and acrylic; dual-CP; ultra-low profile (0.1125λ_0)	- First dual-CP OTA with independent beam control - Broadband ARBW (53.3%) - High transmittance (82.8%) - Ultra-thin (1.125 mm) - Dual beam directions (RHCP/LHCP)

gain of 25.3 dBi, with the main beam in the E-plane directed 15° off-normal. The first sidelobe levels are significantly suppressed, measured at −23.7 dB and −21.1 dB in the H-plane and E-plane, respectively. Across the operational frequency band of 17–22 GHz, the main beam direction remains relatively stable, with a maximum beam squint of less than 0.5°, demonstrating excellent frequency stability. Additionally, the gain fluctuation within this angular direction is minimal, with a deviation of just 0.05 dB. The simulated aperture efficiency is 33.3%, and the antenna achieves a broad simulated 1.5-dB gain bandwidth of 30%, indicating wideband performance with stable radiation characteristics.

TABLE 15. Summary of transparent materials.

Objective	Sustainable Strategy
Substrate sustainability	Use PLA or cellulose-based films.
Conductive transparency	Employ graphene/CNT inks with >80% transparency.
Low-energy processing	Utilize inkjet printing or photonic sintering.
Lifecycle & end-of-life reuse	Design modular, recyclable antenna components.

Figure 19 further corroborates the simulated results with measured data. The main beam is consistently steered 15° off-normal, in agreement with the simulated prediction. At 20 GHz, the measured peak gain is 24.4 dBi—closely matching the simulated value of 25.3 dBi. The measured sidelobe levels are also well suppressed, registering 16.8 dB and 18.7 dB below the main beam in the H-plane and E-plane, respectively. The co-polarization and cross-polarization patterns across the 17–22 GHz range confirm that the RA maintains robust radiation performance and polarization purity, reinforcing its viability for broadband high-gain applications.

The use of heterogeneous materials in the multilayer hybrid dielectric substrates—comprising glass and air—enables a wide phase shift range in the RA element design. At the center frequency of 20 GHz, the element demonstrates a phase variation of up to 494°, with a peak return loss of less than 1.8 dB. An optically TRA based on ITO was designed, fabricated, and experimentally validated, utilizing a F/D ratio of 0.9. The fabricated RA achieves a measured gain of 24.4 dBi, a 1.5 dB gain bandwidth, and maintains a high optical transparency of 75%.

These results confirm the feasibility of realizing high-performance, optically TRA antennas using ITO, offering the combined benefits of broad bandwidth, low return loss, wide phase tuning range, and significant optical transparency.

In [105], a gain enhancement technique is proposed for CubeSat applications, integrating an TRA at a top of solar cells in conjunction with an AIA. Given the limited physical space available on CubeSats, increasing antenna gain within a constrained footprint is particularly challenging. The technique capitalizes on the abundant and renewable solar energy available in space, which is harvested and directed into a quasi-Yagi antenna through a cascaded microwave power amplifier. This configuration enables a gain enhancement of 22.7 dB via the AIA approach. Notably, the AIA also serves as the feed for the TRA, offering two key advantages: an additional 11.0 dB gain and the ability to install the RA directly on existing solar panels, thus eliminating the need for additional structural space.

The proposed architecture consists of three integrated sections: an AIA section, a RA section, and a power management module. A prototype system operating at 25.0 GHz was developed to validate the design. The antenna—measuring 110 × 80 mm^2—achieved a realized gain of 41.3 dB. The TRA was fabricated using ITO patterned on soda-lime glass,

TABLE 16. Classification by conductive material.

Material	Key Features	Performance Metrics	Applications
ITO	High transparency TCO; compatible with many substrates	- Achieves high optical transparency (82%) - Offers 360° phase variation from 12.5–14.5 GHz - Realized gain: 24.3 dBi (offset feed) - High efficiency (41.3%) and low return loss (2.8 dB)	92% transparency (Rogers), up to 25.8 dBi gain, 15% BW; up to 494° phase shift in multilayer design
AgHT-8	Silver-coated film; good for low-profile use	88% light transmittance, gain: 0.64–1.2 dBi, 62–83% efficiency; BW: 10.2–23.92 GHz	WLAN, ISM, 5G
Silver / Ag Nanowires	High conductivity and transparency; scalable via screen-printing	85% transparency, gain: 3–19 dBi (wideband), 11.6 dBi (60 GHz), ~50% efficiency	RFID, wearable, automotive, aerospace
Fluorine-doped Tin Oxide	Durable TCO; excellent environmental stability	80–90% transparency, gain: up to 5.14 dBi (5 GHz), up to 59.78% efficiency at THz	Outdoors, photovoltaic, vehicular, THz
Composite Materials	Multi-layer thin films; balances flexibility, RF, and optical properties	~86% transparency, gain: 1.66 dBi (2.4 GHz); similar at MHz	Wearable, IoT, flexible electronics
Other Materials	Includes water/ethyl acetate, MMMC, GZO, LC-based with mesh	100% transparency (water), 90% (GZO), gains up to 14.35 dBi (LC), wide BW; beam steering to ±50°	Smart windows, THz, eco-friendly, reconfigurable

TABLE 17. Classification by structural characteristics.

Structure Type	Key Characteristics	Performance Metrics	Notable Examples
Single-Layer RA	Minimal thickness; lithography enables precise control	Gain: 33.66 dBi at 400 GHz	FTRA at THz frequencies
Multilayer Hybrid	Air gaps and quartz/glass combos reduce loss and enhance bandwidth	494° phase shift at 20 GHz, 24.4 dBi gain, 75% transmittance	ITO on hybrid quartz structure
Mesh-Type RA	Uses metallic mesh or SSPP tech; low RCS and directional radiation	Gain: 24.5 dBi at 9.6 GHz, sidelobe suppression >15 dB	Low-RCS/stealth communication systems
Fine Metal Line (FML)	High-precision lines via photolithography; wide phase shift and transparency	360° phase shift, >82% transparency, 23.89 dBi gain	Pencil beam reflector antenna

TABLE 18. Classification by functionality.

Application Focus	Key Traits	Performance Metrics	Use Cases
High-Frequency (mmW/THz)	Small form factor, precise lithography needed	33.66 dBi gain at 400 GHz (THz FTRA)	5G, 6G, satellite, THz comms
Solar-Energy Integration	Transparent RA allows light to pass through to photovoltaic cells	41.3 dB realized gain @ 25 GHz with solar harvesting and AIA	CubeSat, self-powered comm systems
Reconfigurable / Beam-Steering	Dynamic beam control via LC or tunable elements	±50° beam steering, 14.35 dBi gain @ 27.5 GHz, 260° phase shift	Adaptive 5G/6G arrays
Low RCS / Stealth	Uses SSPP or special meshes for radar invisibility while maintaining gain	High radiation efficiency, beam control, low radar signature	Defense, drone-based secure comms

and despite the integration of RF and photovoltaic functionalities, the onboard electronics remained fully operational through the incorporated power management system.

As illustrated in Figure 21, the unit cell structure comprises two ITO-based layers separated by a thin air spacer with a thickness of 0.01 mm. The chosen substrate is soda-lime glass, characterized by a ε_r of 7.2 and a tanδ of 0.02, with a total thickness of 0.7 mm. ITO is employed as the radiating layer. It is deposited with a thickness of 1.2 μm and exhibits a conductivity of $\sigma = 2.4 \times 105$ S/m.

This configuration is designed to achieve a balance between optical transparency, electrical performance, and mechanical stability, making it highly suitable for TRA applications.

At the operating frequency of 25.0 GHz, the measured and simulated reflection coefficients are −13.4 dB and −12.4 dB, respectively, as depicted in Figure 22. These values indicate that approximately 94.2% and 95.4% of the input power is effectively received by the antenna, confirming minimal power loss despite a slight frequency shift observed in the measurements. The strong agreement between the experimental and simulated trends validates the accuracy of the design and modeling. Furthermore, the main beam of the complete antenna sub-system remains directed toward the broadside, demonstrating stable radiation characteristics. These results confirm that the proposed antenna sub-system is capable of achieving the desired directional performance while simultaneously offering enhanced gain.

TABLE 19. Classification by sustainability characteristics.

Sustainability Focus	Description	Examples/Benefits
Recyclable Substrates	Use of PLA, cellulose for compostable structures	Biodegradable antennas; environmental compatibility
Carbon-Based Conductors	Graphene, CNTs for lower-impact transparent conductors	Competitive electrical/optical properties; eco-friendly alternatives to ITO
Low-Energy Fabrication	Printing/sintering at low temperatures to reduce energy cost	Inkjet, screen printing enable additive manufacturing
Modular Design	Easily detachable or replaceable components for recycling or repair	Supports green design and long-term usability

Table 13 below highlights for the multilayer ITO based RA:

E. FINITE METAL LINE

The study presented in [103] introduces a highly optically TRA antenna based on a fine metal line (FML) construction technique, aiming to achieve broad phase variation, low return loss, and high optical transparency for use in emerging transparent communication technologies. Utilizing a photolithographic fabrication process to realize the FML patterns, this approach offers precise control over the geometrical features of the radiating elements. The proposed design shows promising potential for integration into applications such as smart windows and AR display systems, where transparency and electromagnetic performance must be simultaneously optimized. The FML methodology enables the development of TRAs without compromising key performance parameters, thereby contributing to the advancement of multifunctional optoelectronic platforms.

Novel Methodologies:

- *Combining Dual-Metasurface and Rasorber*: To achieve low RCS, the study proposes a folded RA design that integrates a frequency selective rasorber (FSR), a diffusion metasurface, and a polarization-conversion focusing metasurface. This configuration enables effective RCS reduction while maintaining high-gain radiation performance.
- *Use of Fine Metal Line (FML) for wideband Structure*: This study utilizes a TRA element based on a FML structure to simultaneously achieve low return loss, high optical transparency, and wide phase variation. The element demonstrates a peak return loss of 2.8 dB and a full 360° phase shift range over the 12.5–14.5 GHz frequency band.
- *Enhancement of Optical Transmittance:* The study shows that the proposed FML structure achieves an optical transmittance exceeding 82%. Future work may focus on optimizing the transmittance further without degrading the RA performance, potentially by exploring alternative materials or modifying the FML geometry.

The proposed RA element, designed for high optical transmittance, comprises three main components: a transparent FML pattern, a quartz glass substrate ($\varepsilon_r = 3.75$, $\tan\delta = 0.0004$), and a transparent ITO ground plane with a sheet resistance of 6 Ω/sq. As depicted in Figure 23(a), this multilayer structure ensures optical transparency. Figure 23(b) details the FML pattern layout, featuring a metal cross and a folded square ring with a linewidth $g \leq 50$ μm, optimized for electromagnetic and optical performance.

Figure 25 presents the realized gain of the proposed pencil beam reflector antenna across the frequency range. Experimental results show that, under a normal feed configuration, the antenna achieves a peak gain of 23.89 dBi at the central frequency of 13.5 GHz, with a half-power beamwidth (HPBW) of 10.3° in the E-plane. The sidelobe levels (SLL) are 20 dB in the E-plane and 18.2 dB in the H-plane. The total efficiency under this configuration is 37.6%. In the offset feed scenario, the maximum gain increases to 24.3 dBi, accompanied by an improved overall efficiency of 41.3%.

- *Liquid Crystal & Transparent Metal Mesh Line*

A novel approach for developing an optically transparent beam-steering antenna is proposed in [100]. Recently, fixed-beam transparent RAs have been investigated for the incorporation of solar panels in [1], [25], and [128]. It utilizing the combined properties of liquid crystal (LC) technology and a transparent metal mesh to realize the first reconfigurable TRA. Since the permittivity of LCs is anisotropic and inhomogeneous under the influence of nonuniform electric and RF fields, accurate modeling begins with analyzing the LC director distribution. Electromagnetic simulations are used to convert this data into permittivity tensors across the LC volume. A simplified model treats the LC as a homogeneous dielectric block with effective permittivity derived for GT7 LC material. A 10 × 10 RA prototype is fabricated and evaluated. The unit cell achieves a phase shift of 260° with a voltage change from 0 to 40 V. Beam steering measurements show E-plane scan from −10° to 50° and H-plane scan from −50° to 50°, with a peak gain of 14.35 dBi. The prototype's optical transparency is also confirmed. The study highlights the trade-offs in RF-optical LC integration and confirms the feasibility of LC-based transparent reconfigurable antennas for advanced multifunctional applications.

- *Transparent Conductive Metal Mesh*

Metal mesh technology offers a promising solution for achieving optically transparent conductive surfaces [126]. It involves selectively etching a metallic sheet to permit the transmission of optical waves while retaining conductive metal pathways for electromagnetic (EM) currents. In this work, the metallic mesh structure, shown in Figure 26(a), features a copper layer with a thickness of 1.2 μm—three times the skin depth of copper (0.39 μm) at 28 GHz—ensuring sufficient EM conduction. For these parameters, the equivalent

sheet resistance and optical transparency are calculated as Rs = 0.11 Ω/sq and Tmesh = 87.1%, respectively.

LC, characterized by anisotropic permittivity in the x, y, and z directions, can be externally modulated via electric or magnetic fields. Figure 26(b) illustrates a standard LC cell configuration, where the LC material is confined between two metal electrodes driven by a voltage source. In its nematic phase, the rod-like LC molecules exhibit partial orientational order, with the average alignment direction defined by directors (n).

By combining the transparent attributes of metal mesh and LC, reconfigurable transparent unit cells can be realized. Traditional LC-based RAs typically comprise arrays of such unit cells [113], [114], [115] assuming uniform electrostatic fields across the cell for modeling purposes. In this study, a unit cell is fabricated using two copper-coated glass substrates enclosing the LC cavity. During simulation, the bias line is neglected to simplify modeling, as its narrow 15 μm width leads to high resistance and can be connected to the patch at the field null point.

To assemble the LC cavity, GT7 LC is injected using capillary force, and the structure is sealed with UV glue. An optical fiber with a cladding diameter of 160 μm assists the process. The completed sample, shown in Figure 27(a), appears slightly milky to yellow due to UV exposure during assembly, which alters the native light milky color of GT7. Applying UV protective coatings can mitigate this effect. Figure 27(b) provides an enlarged view of the patch layer positioned above the ITO ground plane.

Figures 28(a) and 28(b) illustrate the beam-steering radiation patterns at the lower, center, and higher frequencies across the operating bandwidth in both the E-plane and H-plane. In the E-plane, the primary beam can be steered from $-10°$ to $-50°$, with a 3-dB gain drop from the peak observed around $\theta = 20°$, corresponding to a realized gain of 14.35 dBi at the center frequency of 27.5 GHz. In the H-plane, the 3-dB beam-scanning range extends to $\pm 50°$, where the gain varies from 13.65 dB to 10.5 dB. The radiation patterns at the outer frequencies maintain a beamwidth corresponding to a 3-dB drop over approximately 1.5 GHz bandwidth. Throughout the scanning range, the measured and simulated gain values differ by about 1.5–2 dB, attributed to fabrication imperfections and inaccuracies in the measured free-space phase-voltage relationship.

- *Using Anisotropic Impedance Surface Dual-CP*

The paper [107] presents a novel design of an optically TRA antenna that supports dual-CP and operates in the Ka-band. It utilizes an anisotropic impedance surface (AIS) composed of FML on a PET/acrylic/ITO multilayer structure, achieving high optical transparency (82.8%) and a very thin profile ($0.1125\lambda_0$). By combining dynamic phase and Berry phase principles, the unit cell achieves full 360° phase coverage for both right-hand and left-hand circularly polarized (RHCP and LHCP) waves without altering their handedness. The design allows for independently steerable beams for each polarization and ensures strong polarization isolation, making it well-suited for satellite communications in complex electromagnetic environments.

Figure 29 illustrates the structural configuration of the proposed optically TRA unit cell. As shown in Figure. 29(a), the unit cell comprises three dielectric layers stacked vertically: a 0.125 mm thick PET substrate that supports the FML pattern, a 0.5 mm acrylic spacer to maintain mechanical stability, and a 0.5 mm ITO film at the bottom serving as the transparent ground plane. The FML pattern, detailed in Figure. 29(b), is fabricated from 2 μm thick copper and features a symmetrical layout consisting of elliptical, rectangular, and arc-shaped segments strategically designed for dual-CP response. The pattern enables phase manipulation through geometric variation of features such as Rec_l2, Ell_r1/r2, and angle θ.

The full unit cell extents 2.2 mm × 2.2 mm, corresponding to $0.22\lambda_0 \times 0.22\lambda_0$ at 30 GHz, with an overall height of 1.125 mm ($0.1125\lambda_0$), as depicted in Figure. 29(c). Simulations were performed using ANSYS HFSS with Floquet ports to analyze the scattering behavior under periodic boundary conditions. The fabricated RA contains 8400 finely patterned cells and demonstrates strong agreement between simulated and measured results. Key performance metrics include a peak gain of 32.42 dBic, axial ratio bandwidth of 53.3%, and 3-dB gain bandwidths of 33.7% and 30.3% for RHCP and LHCP, respectively. The results confirm the antenna's ability to generate dual-CP beams with high aperture efficiency (up to 34.3%) and stable performance under oblique incidence. Compared to prior works, this design is the first to realize a dual-CP optically TRA with independent beam control, while maintaining high transparency and a low-profile structure.

The optical and RF performance of the fabricated prototype demonstrates the viability of the proposed approach for transparent antenna applications in future 5G and 6G systems. Despite exhibiting higher losses compared to conventional transparent metal mesh without LC or standard opaque LC unit cells, the RA maintains proper functionality. However, further research is essential to address these limitations. Future work may focus on exploring alternative low-loss unit cell configurations, developing new LC materials with reduced loss tangents, and optimizing the design of the metal mesh structure to enhance overall performance.

IV. SUSTAINABLE AND ECO-FRIENDLY MATERIALS ROADMAP FOR TRANSPARENT REFLECTARRAY ANTENNAS

With the increasing deployment of TRAs in consumer, automotive [127], and satellite systems, environmental sustainability is becoming a vital design consideration. Conventional materials like ITO, silver nanowires (AgNW), and PET substrates pose concerns over resource scarcity, recyclability, and manufacturing energy consumption. To address this, the following roadmap outlines eco-conscious alternatives:

A. RECYCLABLE AND BIODEGRADABLE SUBSTRATES

Biodegradable materials such as polylactic acid (PLA) and cellulose-based films are attractive alternatives to traditional plastics. PLA substrates can be processed at low temperature and with non-toxic lithographic or printing techniques, offering potential for compostable or fully recyclable TRAs while maintaining suitable dielectric properties [116], [117], [125].

B. CARBON-BASED TRANSPARENT CONDUCTORS

Alternatives to ITO and AgNW include graphene and carbon nanotube (CNT)-based materials, which demonstrate competitive conductivity ($\sim 10^3$–104 S/m) and transparency (>80%), with lower environmental impact and enhanced flexibility [114], [118]. For example, MWCNT-doped fluorine tin oxide demonstrates enhanced conductivity (∼5 Ω/S) and 77% optical transparency—sufficient for many antenna applications.

C. LOW-ENERGY FABRICATION METHODS

Processes such as inkjet printing, screen printing, and photonic sintering facilitate additive manufacturing of antennas at low thermal budgets. These methods eliminate the need for vacuum deposition or high-temperature sintering, enabling compatibility with biodegradable substrates and significantly reducing energy consumption [119].

D. MODULAR & RECYCLABLE DESIGN

Designing TRA elements as modular, separable components—e.g., detachable meshes or reusable antenna panels—supports component-level recycling and ease of repair. Conducting Life Cycle Assessments (LCA) on material choices further supports environmentally responsible system design [116], [117]

Below Table 15 highlights the objectives and the sustainability for the transparent material use for TRA.

V. CONCLUSION

This review highlights the recent advancements in TRA antennas, focusing on their structural innovations, material developments, and performance optimization across the millimeter-wave and terahertz frequency bands. Various design strategies, such as folded configurations, dual-layer unit cells, FML constructions, and LC-based reconfigurable structures, have demonstrated wide phase tunability, low return loss, and high optical transparency. The integration of materials like quartz, ITO, and soda-lime glass, along with fabrication techniques such as photolithography, has enabled the realization of optically TRAs suitable for compact, high-performance applications in satellites, smart windows, 6G systems, and wearable electronics.

While the results are promising, challenges such as transmission loss, limited bandwidth, and fabrication complexity remain. Future work should focus on optimizing unit cell geometries, improving LC material properties, and exploring hybrid reconfigurable designs to achieve higher efficiency and wider bandwidth. Overall, TRAs represent a critical step toward multifunctional, aesthetically integrated wireless systems for next-generation communication technologies.

TRAs can be classified based on various characteristics, particularly the conductive materials used, which profoundly influence their performance, transparency, and intended applications. Other distinguishing characteristics include their structural designs, operating frequency bands, and advanced functionalities like reconfigurability and integration with other systems.

The following are the Tables in a nutshell for the classification of the conductive materials, structural characteristics, functionality and sustainability:

ACKNOWLEDGMENT

The author would also like to thank Universiti Teknikal Malaysia Melaka (UTeM) for support under the Kesidang Scholarship. They would also like to thank the Staff of UTeM for technical support.

REFERENCES

[1] C. Kocia and S. V. Hum, "Design of an optically transparent reflectarray for solar applications using indium tin oxide," *IEEE Trans. Antennas Propag.*, vol. 64, no. 7, pp. 2884–2893, Jul. 2016, doi: 10.1109/TAP.2016.2555338.

[2] M. Islam and S. Jin, "An overview research on wireless communication network," *Adv. Wireless Commun. Netw.*, vol. 5, no. 1, pp. 19–28, 2019.

[3] M. M. Tawfik, M. F. A. Sree, M. Abaza, and H. H. M. Ghouz, "Performance analysis and evaluation of inter-satellite optical wireless communication system (IsOWC) from GEO to LEO at range 45000 km," *IEEE Photon. J.*, vol. 13, no. 4, pp. 1–6, Aug. 2021.

[4] K. Ramahatla, M. Mosalaosi, A. Yahya, and B. Basutli, "Multiband reconfigurable antennas for 5G wireless and CubeSat applications: A review," *IEEE Access*, vol. 10, pp. 40910–40931, 2022.

[5] Y. Xing and T. S. Rappaport, "Terahertz wireless communications: Co-sharing for terrestrial and satellite systems above 100 GHz," *IEEE Commun. Lett.*, vol. 25, no. 10, pp. 3156–3160, Oct. 2021.

[6] E. Vassos, P. I. Theoharis, S. Chalkidis, F. Tubbal, R. Raad, and A. Feresidis, "A comparative study of a reflectarray antenna based on optical transparent materials," in *Proc. 12th Int. Conf. Modern Circuits Syst. Technol. (MOCAST)*, Jun. 2023, pp. 1–3, doi: 10.1109/MOCAST57943.2023.10176544.

[7] G. Oliveri, F. Zardi, G. Gottardi, and A. Massa, "Optically-transparent EM skins for outdoor-to-indoor mm-wave wireless communications," *IEEE Access*, vol. 12, pp. 65178–65191, 2024.

[8] A. R. Chishti, A. Aziz, M. A. Qureshi, M. N. Abbasi, A. M. Algarni, A. Zerguine, N. Hussain, and R. Hussain, "Optically transparent antennas: A review of the state-of-the-art, innovative solutions and future trends," *Appl. Sci.*, vol. 13, no. 1, p. 210, Dec. 2022.

[9] M. Bhutani, B. Lall, and M. Agrawal, "Optical wireless communications: Research challenges for MAC layer," *IEEE Access*, vol. 10, pp. 126969–126989, 2022.

[10] J. C. Liang, P. Zhang, Q. Cheng, and T. J. Cui, "Reconfigurable intelligent surface with high optical-transparency based on metalmesh," *J. Inf. Intell.*, vol. 1, no. 3, pp. 228–237, Sep. 2023.

[11] J. C. Liang, Y. Gao, Z. W. Cheng, R. Z. Jiang, J. Y. Dai, L. Zhang, Q. Cheng, S. Jin, and T. J. Cui, "An optically transparent reconfigurable intelligent surface with low angular sensitivity," *Adv. Opt. Mater.*, vol. 12, no. 6, Feb. 2024, Art. no. 2202081.

[12] P. Zhang, X. Zhang, and L. Li, "An optically transparent metantenna for RF wireless energy harvesting," *IEEE Trans. Antennas Propag.*, vol. 70, no. 4, pp. 2550–2560, Apr. 2022.

[13] R. B. Green, K. Ding, V. Avrutin, U. Ozgur, and E. Topsakal, "Optically transparent antenna arrays for the next generation of mobile networks," *IEEE Open J. Antennas Propag.*, vol. 3, pp. 538–548, 2022.

[14] W. Jaffray, S. Saha, V. M. Shalaev, A. Boltasseva, and M. Ferrera, "Transparent conducting oxides: From all-dielectric plasmonics to a new paradigm in integrated photonics," *Adv. Opt. Photon.*, vol. 14, no. 2, pp. 148–208, 2022.

[15] G. T. Chavan, Y. Kim, M. Q. Khokhar, S. Q. Hussain, E.-C. Cho, J. Yi, Z. Ahmad, P. Rosaiah, and C.-W. Jeon, "A brief review of transparent conducting oxides (TCO): The influence of different deposition techniques on the efficiency of solar cells," *Nanomaterials*, vol. 13, no. 7, p. 1226, Mar. 2023.

[16] D. A. Ilatovskii, E. P. Gilshtein, O. E. Glukhova, and A. G. Nasibulin, "Transparent conducting films based on carbon nanotubes: Rational design toward the theoretical limit," *Adv. Sci.*, vol. 9, no. 24, Aug. 2022, Art. no. 2201673.

[17] H. Jiang, Y. Zhao, H. Ma, Y. Wu, M. Chen, M. Wang, W. Zhang, Y. Peng, Y. Leng, Z. Cao, and J. Shao, "Broad-band ultrafast all-optical switching based on enhanced nonlinear absorption in corrugated indium tin oxide films," *ACS Nano*, vol. 16, no. 8, pp. 12878–12888, Aug. 2022.

[18] M. O. Daricioglu, C. Durucan, and A. F. Dericioglu, "Functionalization of glass fiber woven fabrics by indium tin oxide (ITO) coatings for electromagnetic wave absorption," *Mater. Sci. Eng., B*, vol. 294, Aug. 2023, Art. no. 116502.

[19] A. Daus, L. Hoang, C. Gilardi, S. Wahid, J. Kwon, S. Qin, J.-S. Ko, M. Islam, A. Kumar, K. M. Neilson, K. C. Saraswat, S. Mitra, H.-S.-P. Wong, and E. Pop, "Effect of back-gate dielectric on indium tin oxide (ITO) transistor performance and stability," *IEEE Trans. Electron Devices*, vol. 70, no. 11, pp. 5685–5689, Nov. 2023.

[20] N. A. Eltresy, A. E. M. A. Elhamid, D. M. Elsheakh, H. M. Elhennawy, and E. A. Abdallah, "Silver sandwiched ITO based transparent antenna array for RF energy harvesting in 5G mid-range of frequencies," *IEEE Access*, vol. 9, pp. 49476–49486, 2021.

[21] L. Cai, J. Zhou, H. Hu, X. Xu, Z. H. Jiang, and W. Hong, "Indium-tin-oxide-based broadband optically transparent reflectarray antenna using a multilayer hybrid dielectric substrate and heterogeneous elements," *IEEE Trans. Antennas Propag.*, vol. 71, no. 11, pp. 9101–9106, Nov. 2023.

[22] Y. Yasuda, Y. Yamada, F. Koshiji, S.-I. Kobayashi, T. Uchida, and Y. Hoshi, "Effect of annealing treatment of indium tin oxide thin films on film properties and transparent antenna properties," *Thin Solid Films*, vol. 794, Apr. 2024, Art. no. 140295.

[23] J.-W. Kim, J.-I. Oh, K.-S. Kim, J.-W. Yu, K.-J. Jung, and I.-N. Cho, "Efficiency-improved UWB transparent antennas using ITO/Ag/ITO multilayer electrode films," *IEEE Access*, vol. 9, pp. 165385–165393, 2021.

[24] A. Sissoko, C. O. Sanogo, and B. Diourté, "A review on conductive and transparent materials used in the design of transparent antennas," *Open J. Antennas Propag.*, vol. 11, no. 2, pp. 11–25, 2023.

[25] J.-J. Peng, S.-W. Qu, and M. Xia, "Optically transparent reflectarray based on indium tin oxide with improved efficiency," *IEEE Trans. Antennas Propag.*, vol. 68, no. 4, pp. 3289–3294, Apr. 2020, doi: 10.1109/TAP.2019.2943408.

[26] C.-T. Wu, Y.-R. Ho, D.-Z. Huang, and J.-J. Huang, "AZO/silver nanowire stacked films deposited by RF magnetron sputtering for transparent antenna," *Surf. Coatings Technol.*, vol. 360, pp. 95–102, Feb. 2019, doi: 10.1016/j.surfcoat.2018.12.105.

[27] Y.-M. Lin, H.-W. Wu, and S.-J. Chang, "Design of LTE/Sub-6 GHz dual-band transparent antenna using frame-structured metal mesh conductive film," *Nanomaterials*, vol. 13, no. 2, p. 221, Jan. 2023.

[28] N.-F. Ren, W.-Z. Wang, B.-J. Li, L.-J. Huang, and Y. Zhang, "Preparation and property optimization of silver-embedded FTO transparent conductive thin films by laser etching and coating AZO layer," *J. Mater. Science: Mater. Electron.*, vol. 32, no. 8, pp. 10644–10661, Apr. 2021.

[29] C. Bianchi, A. C. Marques, R. C. da Silva, T. Calmeiro, and I. Ferreira, "Near infrared photothermoelectric effect in transparent AZO/ITO/Ag/ITO thin films," *Sci. Rep.*, vol. 11, no. 1, p. 24313, Dec. 2021.

[30] P. Li, J. Fleischer, E. Quinn, and D. Park, "Fabrication of an optically transparent planar inverted-F antenna using PEDOT-based silver nanowire clear ink with aerosol-jet printing method towards effective antennas," *J. Manuf. Mater. Process.*, vol. 8, no. 1, p. 39, Feb. 2024.

[31] M. Kundu, "Block copolymer formation and synthesis of fingerprint-patterned AZO nanowires," Master's thesis, Dept. Elect. Eng., College Sci. Eng., Southern Univ. Agricult. Mech. College, Baton Rouge, LA, USA, 2023.

[32] S. Kosuga, K. Suga, R. Suga, T. Watanabe, O. Hashimoto, and S. Koh, "Radiation properties of graphene-based optically transparent dipole antenna," *Microw. Opt. Technol. Lett.*, vol. 60, no. 12, pp. 2992–2998, Dec. 2018, doi: 10.1002/mop.31422.

[33] A. J. A. Al-Gburi, M. M. Ismail, N. J. Mohammed, and T. A. H. Alghamdi, "SAR flexible antenna advancements: Highly conductive polymer-graphene oxide-silver nanocomposites," *Prog. Electromagn. Res. M*, vol. 127, pp. 23–30, Apr. 2024.

[34] S. N. H. Sa'don, M. H. Jamaluddin, A. Althuwayb, and B. Alali, "A review: The influence of graphene material integration in antenna characteristics in the presence of bias for fifth and sixth generation wireless communication application," *Nano Commun. Netw.*, vol. 39, Mar. 2024, Art. no. 100483.

[35] A. Abdelrahman, F. Erchiqui, and M. Nedil, "Preparation and evaluation of conductive polymeric composite from metals alloys and graphene to be future flexible antenna device," *Adv. Mater. Sci.*, vol. 21, no. 4, pp. 34–52, Dec. 2021.

[36] A. Riaz, S. Khan, and T. Arslan, "Design and modelling of graphene-based flexible 5G antenna for next-generation wearable head imaging systems," *Micromachines*, vol. 14, no. 3, p. 610, Mar. 2023.

[37] R. Jain, P. K. Singhal, and V. V. Thakare, "An investigation on unique graphene-based THz antenna," in *Recent Advances in Graphene Nanophotonics*. Cham, Switzerland: Springer, 2023, pp. 163–180.

[38] Q. L. Li, S. W. Cheung, D. Wu, and T. I. Yuk, "Optically transparent dual-band MIMO antenna using micro-metal mesh conductive film for WLAN system," *IEEE Antennas Wireless Propag. Lett.*, vol. 16, pp. 920–923, 2017, doi: 10.1109/LAWP.2016.2614577.

[39] M. N. Abbasi, A. Aziz, K. A. Aljaloud, A. R. Chishti, Y. T. Aladadi, and R. Hussain, "A close proximity 2-element MIMO antenna using optically transparent wired-metal mesh and polyethylene terephthalate material," *IEEE Access*, vol. 11, pp. 78811–78819, 2023.

[40] E. C. Patil, S. Lokhande, U. A. Patil, A. U. Patil, and J. Kumar, "Key components of optically transparent antennas and their specifications," in *Proc. Int. Conf. Microelectron.*, 2024, pp. 81–89.

[41] J. Sun and K.-M. Luk, "Miniature water monopolar patch antenna using transparent high-permittivity liquid substrate," *Electron. Lett.*, vol. 56, no. 10, pp. 475–476, May 2020, doi: 10.1049/el.2020.0159.

[42] A. S. M. Sayem, A. Lalbakhsh, K. P. Esselle, G. Moloudian, J. L. Buckley, and R. B. V. B. Simorangkir, "Advancements, challenges, and prospects of water-filled antennas," *IEEE Access*, vol. 11, pp. 8301–8323, 2023.

[43] H. Abu Bakar, R. Abd Rahim, P. J. Soh, and P. Akkaraekthalin, "Liquid-based reconfigurable antenna technology: Recent developments, challenges and future," *Sensors*, vol. 21, no. 3, p. 827, Jan. 2021, doi: 10.3390/s21030827.

[44] S. Sheikh, M. Shokooh-Saremi, and M.-M. Bagheri-Mohagheghi, "Transparent microstrip patch antenna based on fluorine-doped tin oxide deposited by spray pyrolysis technique," *IET Microw., Antennas Propag.*, vol. 9, no. 11, pp. 1221–1229, Aug. 2015, doi: 10.1049/iet-map.2015.0048.

[45] D. Potti, Y. Tusharika, M. G. N. Alsath, S. Kirubaveni, M. Kanagasabai, R. Sankararajan, S. Narendhiran, and P. B. Bhargav, "A novel optically transparent UWB antenna for automotive MIMO communications," *IEEE Trans. Antennas Propag.*, vol. 69, no. 7, pp. 3821–3828, Jul. 2021, doi: 10.1109/TAP.2020.3044383.

[46] A. S. M. Sayem, A. Lalbakhsh, K. P. Esselle, J. L. Buckley, B. O'Flynn, and R. B. V. B. Simorangkir, "Flexible transparent antennas: Advancements, challenges, and prospects," *IEEE Open J. Antennas Propag.*, vol. 3, pp. 1109–1133, 2022, doi: 10.1109/OJAP.2022.3206909.

[47] S. Lee, S. Pyo, and J.-H. Kim, "Dual-band bidirectional circularly polarized microstrip antenna for CubeSat system," *Microw. Opt. Technol. Lett.*, vol. 60, no. 12, pp. 2989–2992, Dec. 2018, doi: 10.1002/mop.31423.

[48] M. Asif, D. A. Sehrai, S. H. Kiani, J. Khan, M. Abdullah, M. Ibrar, M. Alibakhshikenari, F. Falcone, and E. Limiti, "Design of a dual band SNG metamaterial based antenna for LTE 46/WLAN and Ka-band applications," *IEEE Access*, vol. 9, pp. 71553–71562, 2021, doi: 10.1109/ACCESS.2021.3077844.

[49] M. Cai, Z. Yan, F. Fan, S. Yang, and X. Li, "Double-layer Ku/K dual-band orthogonally polarized high-efficiency transmitarray antenna," *IEEE Access*, vol. 9, pp. 89143–89149, 2021, doi: 10.1109/ACCESS.2021.3089489.

[50] X. Tong, Z. H. Jiang, Y. Li, F. Wu, J. Wu, R. Sauleau, and W. Hong, "An integrated dual-band dual-circularly polarized shared-aperture transmitarray antenna for K-/Ka-band applications enabled by polarization twisting elements," *IEEE Trans. Antennas Propag.*, vol. 71, no. 6, pp. 4955–4966, Jun. 2023, doi: 10.1109/TAP.2023.3263214.

[51] S. Lu and S.-W. Qu, "Low-profile dual-band reflector antenna for high-frequency applications," *Sensors*, vol. 23, no. 13, p. 5781, Jun. 2023, doi: 10.3390/s23135781.

[52] C. M. Lee, Y. Kim, Y. Kim, I. K. Kim, and C. W. Jung, "A flexible and transparent antenna on a polyamide substrate for laptop computers," *Microw. Opt. Technol. Lett.*, vol. 57, no. 5, pp. 1038–1042, May 2015, doi: 10.1002/mop.29011.

[53] W. Hong, S. Lim, S. Ko, and Y. G. Kim, "Optically invisible antenna integrated within an OLED touch display panel for IoT applications," *IEEE Trans. Antennas Propag.*, vol. 65, no. 7, pp. 3750–3755, Jul. 2017, doi: 10.1109/TAP.2017.2705127.

[54] X. Liu, D. R. Jackson, J. Chen, J. Liu, P. W. Fink, G. Y. Lin, and N. Neveu, "Transparent and nontransparent microstrip antennas on a CubeSat: Novel low-profile antennas for CubeSats improve mission reliability," *IEEE Antennas Propag. Mag.*, vol. 59, no. 2, pp. 59–68, Apr. 2017, doi: 10.1109/MAP.2017.2655529.

[55] J. Hautcoeur, L. Talbi, K. Hettak, and M. Nedil, "60 GHz optically transparent microstrip antenna made of meshed AuGL material," *IET Microw., Antennas Propag.*, vol. 8, no. 13, pp. 1091–1096, Oct. 2014, doi: 10.1049/iet-map.2013.0564.

[56] Y. Al-Adhami and E. Erçelebi, "Plasmonic metamaterial dipole antenna array circuitry based on flexible solar cell panel for self-powered wireless systems," *Microw. Opt. Technol. Lett.*, vol. 59, no. 9, pp. 2365–2371, Sep. 2017, doi: 10.1002/mop.30747.

[57] W. An, L. Xiong, S. Xu, F. Yang, H.-P. Fu, and J.-G. Ma, "A Ka-band high-efficiency transparent reflectarray antenna integrated with solar cells," *IEEE Access*, vol. 6, pp. 60843–60851, 2018, doi: 10.1109/ACCESS.2018.2875359.

[58] Y. Yao, W. Chen, X. Chen, and J. Yu, "Design of optically transparent antenna with directional radiation patterns," *Int. J. Antennas Propag.*, vol. 2017, pp. 1–7, 2017, doi: 10.1155/2017/8125432.

[59] A. Martin, O. Lafond, M. Himdi, and X. Castel, "Improvement of 60 GHz transparent patch antenna array performance through specific double-sided micrometric mesh metal technology," *IEEE Access*, vol. 7, pp. 2256–2262, Dec. 2018, doi: 10.1109/ACCESS.2018.2886478.

[60] M. R. Haraty, M. Naser-Moghadasi, A. A. Lotfi-Neyestanak, and A. Nikfarjam, "Transparent flexible antenna for UWB applications," *ACES J.*, vol. 31, no. 12, pp. 1426–1430, 2021.

[61] Y. Kim, C. Lee, S. Hong, C. W. Jung, and Y. Kim, "Design of transparent multilayer film antenna for wireless communication," *Electron. Lett.*, vol. 51, no. 1, pp. 12–14, Jan. 2015, doi: 10.1049/el.2014.3831.

[62] J. Sun and K.-M. Luk, "A wideband low cost and optically transparent water patch antenna with omnidirectional conical beam radiation patterns," *IEEE Trans. Antennas Propag.*, vol. 65, no. 9, pp. 4478–4485, Sep. 2017, doi: 10.1109/TAP.2017.2730250.

[63] Z. J. Silva, C. R. Valenta, and G. D. Durgin, "Optically transparent antennas: A survey of transparent microwave conductor performance and applications," *IEEE Antennas Propag. Mag.*, vol. 63, no. 1, pp. 27–39, Feb. 2021, doi: 10.1109/MAP.2020.2988526.

[64] A. H. Desai and T. Upadhyaya, "Dual-band transparent and non-transparent antennas for wireless application," *Int. J. Electron. Lett.*, vol. 8, no. 2, pp. 170–179, Apr. 2020, doi: 10.1080/21681724.2019.1582703.

[65] A. Desai, T. Upadhyaya, and R. Patel, "Compact wideband transparent antenna for 5G communication systems," *Microw. Opt. Technol. Lett.*, vol. 61, no. 3, pp. 781–786, Mar. 2019, doi: 10.1002/mop.31601.

[66] R. B. Green, M. Toporkov, M. D. B. Ullah, V. Avrutin, U. Ozgur, H. Morkoc, and E. Topsakal, "An alternative material for transparent antennas for commercial and medical applications," *Microw. Opt. Technol. Lett.*, vol. 59, no. 4, pp. 773–777, Apr. 2017, doi: 10.1002/mop.30404.

[67] P. F. S. Júnior, R. C. S. Freire, A. J. R. Serres, S. Y. Catunda, and P. H. D. F. Silva, "Bioinspired transparent antenna for WLAN application in 5 GHz," *Microw. Opt. Technol. Lett.*, vol. 59, no. 11, pp. 2879–2884, Aug. 2017, doi: 10.1002/mop.30853.

[68] R. B. Green, M. Guzman, N. Izyumskaya, B. Ullah, S. Hia, J. Pitchford, R. Timsina, V. Avrutin, U. Ozgur, H. Morkoc, N. Dhar, and E. Topsakal, "Optically transparent antennas and filters: A smart city concept to alleviate infrastructure and network capacity challenges," *IEEE Antennas Propag. Mag.*, vol. 61, no. 3, pp. 37–47, Jun. 2019, doi: 10.1109/MAP.2019.2907895.

[69] H. A. Elmobarak Elobaid, S. K. Abdul Rahim, M. Himdi, X. Castel, and M. Abedian Kasgari, "A transparent and flexible polymer-fabric tissue UWB antenna for future wireless networks," *IEEE Antennas Wireless Propag. Lett.*, vol. 16, pp. 1333–1336, 2017, doi: 10.1109/LAWP.2016.2633790.

[70] S. Anand, D. M. Sudesh, D. S. Kumar, and C. Murthy, "Analysis of titanium-doped indium oxide based optically transparent patch antenna for terahertz communications," *J. Comput. Theor. Nanoscience*, vol. 12, no. 3, pp. 341–344, Mar. 2015, doi: 10.1166/jctn.2015.3734.

[71] P. D. Sowjanya, M. G. N. Alsath, S. Kirubaveni, R. Govindaraj, and N. Santhosh, "Design and experimental evaluation of a proximity coupled transparent patch antenna for WLAN," *IETE J. Res.*, vol. 68, no. 1, pp. 77–84, Jan. 2022, doi: 10.1080/03772063.2019.1588174.

[72] G. Liu, M. R. Dehghani Kodnoeih, K. T. Pham, E. M. Cruz, D. Gonzalez-Ovejero, and R. Sauleau, "A millimeter-wave multibeam transparent transmitarray antenna at Ka-band," *IEEE Antennas Wireless Propag. Lett.*, vol. 18, pp. 631–635, 2019, doi: 10.1109/LAWP.2019.2899925.

[73] M. Stanley, Y. Huang, H. Wang, H. Zhou, A. Alieldin, and S. D. Joseph, "A transparent dual-polarized antenna array for 5G smartphone applications," in *Proc. IEEE Int. Symp. Antennas Propag. USNC/URSI Nat. Radio Sci. Meeting*, 2018, pp. 635–636, doi: 10.1109/APUSNCURSINRSM.2018.8609096.

[74] Y. Goliya, A. Rivadeneyra, J. F. Salmeron, A. Albrecht, J. Mock, M. Haider, J. Russer, B. Cruz, P. Eschlwech, E. Biebl, M. Becherer, and M. R. Bobinger, "Next generation antennas based on Screen-Printed and transparent silver nanowire films," *Adv. Opt. Mater.*, vol. 7, no. 21, Nov. 2019, Art. no. 1900995, doi: 10.1002/adom.201900995.

[75] L. Song, A. C. Myers, J. J. Adams, and Y. Zhu, "Stretchable and reversibly deformable radio frequency antennas based on silver nanowires," *ACS Appl. Mater. Interfaces*, vol. 6, no. 6, pp. 4248–4253, Mar. 2014, doi: 10.1021/am405972e.

[76] Y.-X. Sun, D. Wu, X. S. Fang, and J. Ren, "On-glass grid structure and its application in highly-transparent antenna for Internet of Vehicles," *IEEE Trans. Veh. Technol.*, vol. 72, no. 1, pp. 93–101, Jan. 2023, doi: 10.1109/TVT.2022.3205899.

[77] P. Lunca-Popa, J.-B. Chemin, N. Adjeroud, V. Kovacova, S. Glinsek, N. Valle, M. El Hachemi, S. Girod, O. Bouton, and J. P. Maris, "Study of gallium-doped zinc oxide thin films processed by atomic layer deposition and RF magnetron sputtering for transparent antenna applications," *ACS Omega*, vol. 8, no. 6, pp. 5475–5485, Feb. 2023, doi: 10.1021/acsomega.2c06574.

[78] S. Syed Feroze Hussain and D. Thiripurasundari, "A review on optically transparent antenna fabricated with conductive nano-material oxides," *J. Electron. Mater.*, vol. 51, no. 12, pp. 6707–6734, Dec. 2022, doi: 10.1007/s11664-022-09916-w.

[79] E. C. Patil, S. D. Lokhande, U. A. Patil, A. U. Patil, and J. Kumar, "Optically transparent dual-band antenna for UHF and S-band applications," *Opt. Mater.*, vol. 147, Jan. 2024, Art. no. 114615, doi: 10.1016/j.optmat.2023.114615.

[80] Y. Jiang, H. Li, and M. Rangaswamy, "Adaptive subspace signal detection with uncertain partial prior knowledge: off-grid problem and efficient implementation," *IEEE Trans. Aerosp. Electron. Syst.*, vol. 56, no. 1, pp. 558–571, May 2019.

[81] V. G. D. Kumar, "Tin in applications meeting the green challenge," The University of Malaya Press, Kuala Lumpur, Malaysia, Tech. Rep., 2014.

[82] D. Li, D. Zhang, K. S. Lim, Y. Hu, Y. Rong, A. Mei, N.-G. Park, and H. Han, "A review on scaling up perovskite solar cells," *Adv. Funct. Mater.*, vol. 31, no. 12, 2021, Art. no. 2008621.

[83] Y.-Y. Chang, M.-M. Fan, X.-J. Xu, Y.-D. Wang, and L. Cao, "A fast-speed self-powered ZnS nanoparticles/α-Ga_2O_3 nanorod array/FTO UV photodetector based on a photoeletrochemical cell for outdoor UV detection," *Chem. Phys. Lett.*, vol. 832, Dec. 2023, Art. no. 140879, doi: 10.1016/j.cplett.2023.140879.

[84] A. Bhattacharya, B. Roy, S. K. Chowdhury, and A. K. Bhattacharjee, "Compact slotted UWB monopole antenna with tuneable band-notch characteristics," *Microw. Opt. Technol. Lett.*, vol. 59, no. 9, pp. 2358–2365, Sep. 2017, doi: 10.1002/mop.30730.

[85] S. M. Uddin, M. R. Hossain, M. S. Rabbi, M. A. Hasan, and M. S. Zishan, "Unmanned aerial vehicle for cleaning the high rise buildings," in *Proc. Int. Conf. Robot., Elect. Signal Process. Techn. (ICREST)*, Jan. 2019, pp. 657–661.

[86] V. Manohar and Y. Rahmat-Samii, "Understanding the radiation characteristics of metal-only, low-profile, offset stepped parabolic reflector antennas: Simulation, analysis, and measurement," *IEEE Trans. Antennas Propag.*, vol. 69, no. 8, pp. 5078–5083, Aug. 2021, doi: 10.1109/TAP.2021.3060090.

[87] R. K. Arya, "Reflectarray antenna design," in *RF, Microwave and Millimeter Wave Technologies*, H. Kumar and E. S. Gopi, Eds., Cham, Switzerland: Springer Nature, 2024, pp. 107–118, doi: 10.1007/978-3-031-62526-8_8.

[88] G. Kim, M. Hwang, H. Jeong, C.-M. Lim, K. Y. Park, and S. Kim, "Design of a flat-panel metasurface reflectarray C-band antenna," *Electronics*, vol. 11, no. 17, p. 2729, Aug. 2022, doi: 10.3390/electronics11172729.

[89] D. Martinez-De-Rioja, E. Martinez-De-Rioja, Y. Rodriguez-Vaqueiro, J. A. Encinar, A. Pino, M. Arias, M. Arrebola, and G. Toso, "Parabolic reflectarray antenna to generate multiple beams for geostationary high throughput satellites in Ka-band," *Int. J. Microw. Wireless Technol.*, vol. 15, no. 1, pp. 15–24, Feb. 2023.

[90] P. Nayeri, F. Yang, and A. Z. Elsherbeni, "Introduction to reflectarray antennas," in *Reflectarray Antennas: Theory, Designs, and Applications*, 2018, pp. 1–8, doi: 10.1002/9781118846728.ch1.

[91] S. Xu and F. Yang, "Reflectarray antennas," in *Handbook of Antenna Technologies*, vol. 2. Singapore: Springer, 2016, pp. 1279–1320.

[92] G. K. Soni, D. Yadav, and A. Kumar, "Design consideration and recent developments in flexible, transparent and wearable antenna technology: A review," *Trans. Emerg. Telecommun. Technol.*, vol. 35, no. 1, p. 4894, Jan. 2024, doi: 10.1002/ett.4894.

[93] Y. Morimoto, S. Shiu, I. W. Huang, E. Fest, G. Ye, and J. Zhu, "Optically transparent antenna for smart glasses," *IEEE Open J. Antennas Propag.*, vol. 4, pp. 159–167, 2023, doi: 10.1109/OJAP.2023.3238721.

[94] M. Rohaninezhad, M. Jalali Asadabadi, C. Ghobadi, and J. Nourinia, "Design and fabrication of a super-wideband transparent antenna implanted on a solar cell substrate," *Sci. Rep.*, vol. 13, no. 1, p. 9977, Jun. 2023, doi: 10.1038/s41598-023-37073-5.

[95] T. Yasin, R. Baktur, and C. Furse, "A comparative study on two types of transparent patch antennas," in *Proc. 30th URSI Gen. Assem. Scientific Symp.*, Aug. 2011, pp. 1–4, doi: 10.1109/URSIGASS.2011.6050441.

[96] R. Malia, K. R. Jha, and S. K. Sharma, "Solar cell integrated optically transparent antenna," in *Proc. IEEE Microw., Antennas, Propag. Conf. (MAPCON)*, Mali, Dec. 2023, pp. 1–4, doi: 10.1109/mapcon58678.2023.10463809.

[97] J. Zhou, L. Cai, X. Wang, Z. H. Jiang, and W. Hong, "A design of optically transparent reflectarray based on ITO material," in *Proc. Int. Appl. Comput. Electromagn. Soc. Symp. (ACES-China)*, 2023, pp. 1–3, doi: 10.23919/ACES-China60289.2023.10249520.

[98] J. Ren, R. He, Y.-X. Sun, J. Wang, Y. Wang, J. Liu, H.-H. Zhang, and Y. Yin, "Low-cost and highly-transparent reflectarray using on-glass metal line and ITO grid ground," *Microw. Opt. Technol. Lett.*, vol. 67, no. 2, p. 70126, Feb. 2025.

[99] H.-J. Song and T. Nagatsuma, "Present and future of terahertz communications," *IEEE Trans. Terahertz Sci. Technol.*, vol. 1, no. 1, pp. 256–263, Sep. 2011, doi: 10.1109/TTHZ.2011.2159552.

[100] P. Aghabeyki, P. de la Rosa, M. Caño-García, X. Quintana, R. Guirado, and S. Zhang, "Optically transparent beam-steering reflectarray antennas based on a liquid crystal for millimeter-wave applications," *IEEE Trans. Antennas Propag.*, vol. 72, no. 1, pp. 614–627, Jan. 2024, doi: 10.1109/TAP.2023.3332473.

[101] Z.-W. Miao, Z.-C. Hao, Y. Wang, B.-B. Jin, J.-B. Wu, and W. Hong, "A 400-GHz high-gain quartz-based single layered folded reflectarray antenna for terahertz applications," *IEEE Trans. Terahertz Sci. Technol.*, vol. 9, no. 1, pp. 78–88, Jan. 2019, doi: 10.1109/TTHZ.2018.2883215.

[102] P. Jiang, W. Jiang, and S. Gong, "A mesh-type low RCS reflectarray antenna based on spoof surface plasmon polariton," *IEEE Antennas Wireless Propag. Lett.*, vol. 20, pp. 224–228, 2021, doi: 10.1109/LAWP.2020.3046127.

[103] B. Chen, B. Wu, H.-R. Zu, J.-Q. Hou, and T. Su, "Experimental demonstration of high optically transparent reflectarrays using fine metal line structure," *IEEE Trans. Antennas Propag.*, vol. 70, no. 11, pp. 10504–10511, Nov. 2022, doi: 10.1109/TAP.2022.3195461.

[104] X. W. Dai, Y. H. Zhang, Z. Li, W. Yu, L. Liu, and G. Q. Luo, "Optically transparent circularly polarized reflectarray for Ka-band applications," *IEEE Trans. Antennas Propag.*, vol. 72, no. 6, pp. 5414–5419, Jun. 2024, doi: 10.1109/TAP.2024.3400024.

[105] Y.-S. Chen, Y.-H. Wu, and C.-C. Chung, "Solar-powered active integrated antennas backed by a transparent reflectarray for CubeSat applications," *IEEE Access*, vol. 8, pp. 137934–137946, 2020, doi: 10.1109/ACCESS.2020.3012133.

[106] T.-M. Wong and K.-M. Luk, "A wideband optically transparent reflectarray antenna with circular polarization," *IEEE Antennas Wireless Propag. Lett.*, vol. 24, pp. 2402–2406, 2025, doi: 10.1109/LAWP.2025.3564948.

[107] X. W. Dai, Z. Li, H. Ruan, W. Yu, L. Liu, and G. Q. Luo, "Anisotropic-impedance-surface-based broadband dual-CP polarization optically transparent reflectarray using fine metal line," *IEEE Antennas Wireless Propag. Lett.*, pp. 1–5, 2025, doi: 10.1109/LAWP.2025.3573874.

[108] D. Kundu, A. Parameswaran, H. S. Sonalikar, D. Bhattacharya, and S. Gupta, "A low-RCS circularly polarized reflectarray antenna with a linearly polarized feed," *IEEE Trans. Antennas Propag.*, vol. 71, no. 8, pp. 6501–6512, Aug. 2023, doi: 10.1109/TAP.2023.3269149.

[109] M. K. T. Al-Nuaimi, W. G. Whittow, G.-L. Huang, R.-S. Chen, and S.-W. Wong, "Wideband radar-cross-section reduction using parabolic phased metasurfaces," *IEEE Antennas Wireless Propag. Lett.*, vol. 22, pp. 1547–1551, 2023, doi: 10.1109/LAWP.2023.3250453.

[110] S. Yang, Y. Chang, and B. Li, "A dual-band reflectarray antenna with low radar cross section," in *Proc. Int. Appl. Comput. Electromagn. Soc. Symp. (ACES-China)*, Hangzhou, China, 2023, pp. 1–3, doi: 10.23919/ACES-China60289.2023.10249654.

[111] H. Wen, B. Weng, B. Wang, W. Xiao, X. Liu, Y. Wang, M. Zhang, and H. Huang, "Advancements in transparent conductive oxides for photoelectrochemical applications," *Nanomaterials*, vol. 14, no. 7, p. 591, Mar. 2024, doi: 10.3390/nano14070591.

[112] C. Habis, J. Zaraket, and M. Aillerie, "Transparent conductive oxides. Part II. Specific focus on ITO, ZnO-AZO, SnO2-FTO families for photovoltaics applications," *Defect Diffusion Forum*, vol. 417, pp. 257–272, Jun. 2022, doi: 10.4028/p-6fqmfi.

[113] W. Zhang, Y. Li, and Z. Zhang, "A reconfigurable reflectarray antenna with an 8 μm-thick layer of liquid crystal," *IEEE Trans. Antennas Propag.*, vol. 70, no. 4, pp. 2770–2778, Apr. 2022, doi: 10.1109/TAP.2021.3125378.

[114] G. Perez-Palomino, P. Baine, R. Dickie, M. Bain, J. A. Encinar, R. Cahill, M. Barba, and G. Toso, "Design and experimental validation of liquid crystal-based reconfigurable reflectarray elements with improved bandwidth in F-band," *IEEE Trans. Antennas Propag.*, vol. 61, no. 4, pp. 1704–1713, Apr. 2013, doi: 10.1109/TAP.2013.2242833.

[115] J. Yang, C. Cai, Z. Yin, T. Xia, S. Jing, H. Lu, and G. Deng, "Reflective liquid crystal terahertz phase shifter with tuning range of over 360°," *IET Microw., Antennas Propag.*, vol. 12, no. 9, pp. 1466–1469, Jul. 2018, doi: 10.1049/iet-map.2017.0898.

[116] H. I. Malik, M. Y. Ismail, S. Adnan, S. R. Masrol, and N. Nafarizal, "A wideband reflectarray antenna based on organic substrate materials," *TELKOMNIKA (Telecommunication Comput. Electron. Control)*, vol. 17, no. 1, pp. 8–14, Feb. 2019, doi: 10.12928/telkomnika.v17i1.9593.

[117] J. Kang, H. Kim, K. S. Kim, S.-K. Lee, S. Bae, J.-H. Ahn, Y.-J. Kim, J.-B. Choi, and B. H. Hong, "High-performance graphene-based transparent flexible heaters," *Nano Lett.*, vol. 11, no. 12, pp. 5154–5158, Dec. 2011, doi: 10.1021/nl202311v.

[118] H. Jeon, S. Jin, and K.-Y. Shin, "Highly flexible, high-performance radio-frequency antenna based on free-standing graphene/polymer nanocomposite film," *Appl. Surf. Sci.*, vol. 582, Apr. 2022, Art. no. 152455, doi: 10.1016/j.apsusc.2022.152455.

[119] E. Sipilä, J. Virkki, J. Wang, L. Sydänheimo, and L. Ukkonen, "Brush-painting and photonic sintering of copper oxide and silver inks on wood and cardboard substrates to form antennas for UHF RFID tags," *Int. J. Antennas Propag.*, vol. 2016, pp. 1–8, Jan. 2016, doi: 10.1155/2016/3694198.

[120] Y. Yao, Y. Shao, J. Zhang, and J. Zhang, "High efficiency and high gain indium tin oxide optical transparent antenna based on Fabry–Perot cavity," *Opt. Mater.*, vol. 168, 2025, Art. no. 117395, doi: 10.1016/j.optmat.2025.117395.

[121] B. Dominguez, F. Silva, A. Baghel, D. Albuquerque, and P. Pinho, "Optically transparent antennas for 5G and beyond: A review," *Electronics*, vol. 14, no. 8, p. 1616, Apr. 2025.

[122] Z. Zhou, Y. Zhang, Z. Kuang, Y. Li, and Z. David Chen, "An optically transparent near-zero-index grating metamaterial for enhanced on-glass millimeter-wave radiation," *IEEE Trans. Antennas Propag.*, vol. 73, no. 6, pp. 4092–4097, Jun. 2025.

[123] B. Zhang, W. Hu, F. Yang, S. Xu, and C. Jin, "Integrated low-RCS reflectarray antenna based on multimode metasurface," *IEEE Antennas Wireless Propag. Lett.*, vol. 24, no. 8, pp. 2467–2471, Aug. 2025.

[124] M. K. T. Al-Nuaimi, G.-L. Huang, R.-S. Chen, X. Chen, and A. A. Kishk, "Novel wideband reflectarray antenna supporting multiple vehicle-to-everything (V2X) links," *IEEE Antennas Wireless Propag. Lett.*, pp. 1–5, 2025.

[125] M. Nasir, S. Koziel, and A. Iftikhar, "A miniaturized and high optically transparent frequency selective surface for RF shielding using double-glazed glass windows for green building applications," *IEEE Access*, vol. 13, pp. 18053–18062, 2025.

[126] Y. Yu, Y. Dong, Y. He, and Y.-F. Cheng, "A high-isolation optically transparent 2 × 2 antenna array using metal mesh material," *Micromachines*, vol. 16, no. 5, p. 528, Apr. 2025.

[127] X. Liu, B. Sanz-Izquierdo, S. Gao, Q. Luo, L. Zhang, L. Wen, X.-X. Yang, and L. Wang, "Dual-band dual-polarized array based on electromagnetic transparent antenna for vehicle-mounted base station systems," *IEEE Trans. Veh. Technol.*, vol. 74, no. 7, pp. 10639–10648, Jul. 2025.
[128] H. Kim, B. Moon, S. Bang, S. Oh, and J. Oh, "PCB-based dual-polarized liquid crystal reflectarray with high aperture efficiency and bridge-shaped biasing topology for 2D scanning," *IEEE Access*, vol. 13, pp. 116407–116418, 2025.
[129] B. Kim, S. Bang, S. Kim, D. Kwon, S. Kim, and J. Oh, "Locally optimal periods in periodic optically transparent two-metal-layered refractive metasurfaces for outdoor-to-indoor communication," *IEEE Antennas Wireless Propag. Lett.*, vol. 24, no. 5, pp. 1253–1257, May 2025.
[130] Y. Cai, Y. Dai, Y. Ma, G. Wang, G. Xu, X. Ren, H. Wang, X. Zhao, and X. Wu, "Optically transparent transmissive orbital angular momentum (OAM) metasurface with high transmittance and broadband characteristics," *Opt. Exp.*, vol. 33, no. 12, p. 24385, Jun. 2025.
[131] Y. S. Gurbet and S. Doğu, "Comprehensive review of Ku, K, and Ka band antenna designs: Applications in CubeSats," *Int. J. Aeronaut. Space Sci.*, pp. 1–50, Jun. 2025.

ALTAF AHMED MUGHERI received the B.E. degree in electronics engineering from SSUET, in 2009, and the M.E. degree in telecommunication engineering from the NED University of Engineering and Technology, Karachi, Pakistan, in 2019. He is currently pursuing the Ph.D. degree from UTeM, Malaysia. He served as a Senior Lecturer at the Department of Electronic Engineering, Dawood University of Engineering and Technology, Karachi, Pakistan. With over ten years of academic experience, his teaching and research interests include antenna design, microwave engineering, and RF. He has actively participated in national and international conferences. His current research interests include reflectarray antenna structures, FSS, and RIS. He continues to contribute actively to the field of electronics and communication engineering.

MUHAMMAD INAM ABBASI (Senior Member, IEEE) received the B.Sc. degree in electrical engineering (telecommunication) from the Centre for Advanced Studies in Engineering (CASE Islamabad), University of Engineering and Technology (UET), Taxilla, Pakistan, in 2008, and the Master by Research and Ph.D. degrees in electrical engineering from Universiti Tun Hussein Onn Malaysia (UTHM), in 2011 and 2016, respectively. He joined the Wireless and Radio Science Centre (WARAS), Universiti Tun Hussein Onn Malaysia (UTHM), as a Graduate Research Assistant, in 2009. He was a Postdoctoral Research Fellow at the Wireless Communication Centre (WCC), Universiti Teknologi Malaysia (UTM), from 2017 to 2018. Currently, he is a Senior Lecturer with the Faculty of Electrical and Electronic Engineering Technology, Universiti Teknikal Malaysia Melaka (UTeM). He has published one book and more than 80 research papers in internationally indexed journals and conferences. His research interests include high-performance planar and printed antenna design, passive and reconfigurable reflectarray and planar reflector antennas, and novel materials for the design of enhanced performance antennas.

IMRAN MOHD IBRAHIM (Senior Member, IEEE) received the bachelor's, master's, and Ph.D. degrees in electrical engineering from Universiti Teknologi Malaysia, in 2000, 2005, and 2016, respectively. He is currently an Associate Professor with Universiti Teknikal Malaysia Melaka. He served as the Faculty's Inaugural Deputy Dean (research and postgraduate study) and contributed to the early development of research activities at the faculty and institution. He serves as a Drafter os the technical code, prediction, and measurement of RF-EMF exposure from base stations. He has led several grants from industry, government, and the university in antenna research and wireless communication. He has published more than 100 journals and conference papers. His research interests include antenna and microwave device design. He has supervised the Ph.D. and master's students by research in antenna design for beyond 5G and medical applications. He was elevated to an IEEE Senior Membership, in 2021, based on his significant contributions in the electrical and electronic engineering field. He is a Committee Member of IMT and the Future Networks Working Group under Malaysia Technical Standard Forum Berhad. In January 2023, he was appointed as the TVET Ambassador of UTeM, for the Project Knowledge Transfer and Mobile Wifi Router Installation for Rural School Area.

SAAD HASSAN KIANI received the B.S. degree from the City University of Science and Information Technology, in 2014, the M.S. degree from Iqra National Uuniversity, in 2018, and the Ph.D. degree from the IIC University of Technology, Cambodia, in 2022. He was a part of the Smart Systems Engineering Laboratory, College of Engineering, Prince Sultan University, Saudi Arabia, from July 2022 to January 2023. He was a Research Scientist (remote) with the RF Microsense Research Group, Istanbul Medipol University, Istanbul, Türkiye, and the Advanced Electromagnetics Research Group, King Abdulaziz University, Jeddah, Saudi Arabia, from 2023 to 2024. Currently, he is a Postdoctoral Researcher with the Fakulti Teknologi dan Kejuruteraan Elektronik dan Komputer (FTKEK), Universiti Teknikal Malaysia Melaka (UTeM), Malaysia. His research interests include MIMO antenna systems, slot antennas, origami and Kirigami antennas, multiband antennas, implantable antennas, frequency-selective surfaces, and metasurfaces.

MUHAMMAD HASHIM DAHRI received the Bachelor of Engineering degree in telecommunications from the Mehran University of Engineering and Technology (MUET), Pakistan, in 2010, the Master by Research degree in electrical engineering from Universiti Tun Hussein Onn Malaysia (UTHM), in 2014, and the Ph.D. degree from the Wireless Communication Centre (WCC), Universiti Teknologi Malaysia (UTM), in 2019. He was a Postdoctoral Research Fellow at the Faculty of Electrical and Electronic Engineering, Universiti Tun Hussein Onn Malaysia (UTHM). Currently, he is an Assistant Professor with the Dawood University of Engineering and Technology, Karachi, Pakistan. He has published more than 20 research papers in various indexed journals and conference proceedings. His research interests include reflectarray antennas, planar printed antennas, and tunable materials for antenna design.

MUHAMMAD RAMLEE KAMARUDIN (Senior Member, IEEE) received the degree (Hons.) in electrical and telecommunication engineering from Universiti Teknologi Malaysia, Johor Bahru, Malaysia, in 2003, and the MSc degree in communication engineering and the Ph.D. degree in electrical engineering from the University of Birmingham, Birmingham, U.K., in 2004 and 2007, respectively, under the supervision of Emeritus Prof. Peter Hall. He is currently a Professor with the Faculty of Electrical and Electronic Engineering, Universiti Tun Hussein Onn Malaysia. Prior to this appointment, he was a Senior Lecturer with the Centre for Electronic Warfare, Information and Cyber, Cranfield Defense and Security, Cranfield University, U.K., and an Associate Professor with the Wireless Communication Centre, Universiti Teknologi Malaysia. He holds a SCOPUS H-Index of 23 with over 2000 citations. He has authored a book chapter of a book titled *Antennas and Propagation for Body-Centric Wireless Communications* and has published over 240 technical papers in leading journals and international proceedings, including IEEE Transaction on Antennas and Propagation, IEEE Antennas and Wireless Propagation Letter, *IEEE Antenna Magazine*, IEEE Access, *International Journal of Antennas and Propagation*, *Progress in Electromagnetic Research*, *Microwave and Optical Technology Letters*, and *Electronics Letters*. His research interests include antenna design for 5G/6G, MIMO antennas, array antennas for beam-forming and beam steering, wireless on-body communications, in-body communications (implantable antenna), RF and microwave communication systems, and antenna diversity. He is a member of IET, the IEEE Antennas and Propagation Society, the IEEE Communication Society, the IEEE Microwave Theory and Techniques Society, and the IEEE Electromagnetic Compatibility Society; an Executive Member of the Antenna and Propagation, Malaysia Chapter; an Associate Editor of *Electronics Letters* and *IET Microwaves, Antennas and Propagation*; and an Academic Editor of *International Journal of Antennas and Propagation*.

ZAID AHMED SHAMSAN (Senior Member, IEEE) received the B.Sc. degree (Hons.) in electronics and communication engineering from Sudan University of Sciences and Technology (SUST), in 2002, and the master's and Ph.D. degrees from Universiti Teknologi Malaysia (UTM), Malaysia, in 2007 and 2010, respectively. Since 2003, he has been with the Faculty of Engineering and Information Technology, Taiz University, Yemen. He was a Postdoctoral Research Fellow with the Wireless Communication Center (WCC), from April 2010 to April 2012. He is currently a Full Professor with the Department of Electrical Engineering, College of Engineering, Imam Mohammad Ibn Saud Islamic University (IMSIU), Saudi Arabia, where he heads the International Publishing Unit (IPU). He is interested in teaching courses, such as wireless mobile communication, satellite communication, and digital signal processing. He has published several scientific papers in high-impact factor and archival technical journals and conferences. His research interests include 4G, 5G, and 6G systems, LMDS system analysis, interference analysis techniques, mathematical modeling for coexistence analysis in wireless networks and frequency spectrum management, wave propagation and antenna, rainfall and dust storm analysis and mitigation, and free space optics.

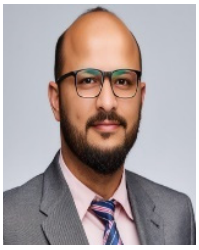

QAMMER HUSSAIN ABBASI (Senior Member, IEEE) is currently a Professor of applied electromagnetics and sensing with the James Watt School of Engineering, the Executive Director of the Communication Sensing and Imaging Hub, and the School Theme Lead of connecting people priority with the University of Glasgow, U.K. He has grant portfolio of more than £12m and contributed to more than 450 leading international technical journals and peer-reviewed conference papers (including nature portfolio) and 11 books and received several recognitions for his research, including the URSI Young Scientist Awards, in 2019, the U.K. Exceptional Talent Endorsement by the Royal Academy of Engineering, the Sensor Young Scientist Award, in 2021, the World Class Professor by Indonesian Ministry, in 2022, the National Talent Pool Award by Pakistan, the International Young Scientist Award by NSFC China, the University Research Excellence Award, the Research Culture Award Commendation, in 2021, the University Wide Teaching Excellence Awardat Glasgow, in 2022, 11 best paper awards, the 2021 Best Chapter Award as the Chair from IEEE APS and IEEE MTT both, Named one of the top 100 influential voices in 5G as per the June 2022 report "Who is Who in 5G?" by Analytica as few examples. In addition, his work received Media Coverage by Analog IC Tips, Microwaves and RF Newsletters, Vertical News, BBC News, Scotland TV, Fiercewireless, and many other media houses around the world. He is a fellow of European Alliance of Innovation, the Royal Society of Arts, and the Institution of Engineering and Technology (IET). He was an Industrial Fellow of the Royal Academy of Engineering, from 2022 to 2023. He is/was a Committee Member for the IEEE APS Young Professional; the Sub-Committee Chair of the IEEE YP Ambassador Program, IEEE 1906.1.1 Standard on Nano Communication, IEEE APS/SC WG P145, and IET Antenna and Propagation and Healthcare Network; and the Union of Radio Science Commission B U.K. Representative. He has been a member of the technical program committees of several IEEE flagship conferences and technical reviewer for several IEEE and top notch journals and acted as the TPC Chair and the Executive Chair for 4th, 5th and 6th international UCET Conference, in 2019, 2020, and 2021; the General Chair of EAI Bodynets 2021; and the Local Organizing Chair of IEEE WCNC 2023, EUCAP 2024, and ICC 2026. He is an Associate Editor for IEEE Journal of Electromagnetics, RFand Microwaves in Medicine and Biology, IEEE Sensors Journal, IEEE Internet of Things Journal, IEEE Open Journal of Antenna and Propagation, and *Scientific Reports*.